NASA CONTRACTOR REPORT

NASA CR-916

THE APPLICATION OF HIGH TEMPERATURE RADIATIVE THERMAL CONDUCTIVITY OF MINERALS AND ROCKS TO A MODEL OF LUNAR VOLCANISM

Prepared by
ARTHUR D. LITTLE, INC.
Cambridge, Mass.
for Manned Spacecraft Center

NATIONAL AERONAUTICS AND SPACE ADMINISTRATION • WASHINGTON, D. C. • NOVEMBER 1967

NASA CR-916

THE APPLICATION OF HIGH TEMPERATURE RADIATIVE THERMAL CONDUCTIVITY OF MINERALS AND ROCKS TO A MODEL OF LUNAR VOLCANISM

Prepared under Contract No. NAS 9-5840 by
ARTHUR D. LITTLE, INC.
Cambridge, Mass.

for Manned Spacecraft Center

NATIONAL AERONAUTICS AND SPACE ADMINISTRATION

For sale by the Clearinghouse for Federal Scientific and Technical Information
Springfield, Virginia 22151 – CFSTI price $3.00

TABLE OF CONTENTS

LIST OF TABLES

LIST OF FIGURES

I. BACKGROUND

The results of a recent study [McConnell et al., 1965] [McConnell et al., 1967] indicated that the thermal conductivity of rocks and minerals is insufficiently well known, under the conditions of temperature and pressure in the interior of the moon, to be able to predict magma generation, migration, and crystallization adequately.

At the relatively high temperatures that probably exist deep in the lunar interior, heat flow takes place by both lattice conduction and radiative transfer. The radiative transfer which should be dominant at the higher temperatures is caused by a process of repeated emission and re-absorption of radiation modified by the effect of scattering by discontinuities such as inclusions or grain boundaries. The rate of emission depends on the blackbody spectral distribution at the temperature of the medium and on the optical constants n and k of the medium which are, in general, strong functions of the wavelength. The rate of re-absorption also depends on n and k. The scattering depends on the size and spatial distribution of the discontinuities in n and k.

This mechanism of heat transfer has been extensively discussed for hot glass [Gardon, 1961] [Kellet, 1952] [Czerny and Genzel, 1952] and ceramic materials [Lee and Kingery, 1960]. These authors have considered that the thermal conductivity of any substance is effectively the sum of the ordinary phonon conductivity and the radiative conductivity. They obtain simple expressions for the radiative term of the form:

$$C_r = \frac{16}{3} \frac{n^2 \sigma T^3}{\alpha} \qquad (1)$$

by considering the material to be gray. Here n is the refractive index, σ is the Stefan-Boltzmann constant, T the absolute temperature and α is the absorption coefficient. The assumption of grayness means simply that α is independent of wavelength, finite, and nonzero.

In this approximation, the T^3 behavior of the radiative conductivity (neglecting the temperature dependences of n and α) when contrasted with the T^{-1} behavior of ordinary thermal conductivity above the Debye

temperature, shows that at high temperatures the radiative conductivity should be predominant. Clark [1957a] and others have applied the radiative transfer concept to the thermal history of the earth. Clark derived a relationship for the radiative conductivity

$$C_r = \frac{4}{3} \int_0^\infty \frac{n^2(\lambda,T)}{\varepsilon(\lambda,T)} \frac{B(\lambda,T)}{\partial T} \, d\lambda \qquad (2)$$

where ε is the extinction coefficient, B is the blackbody function, and λ the radiation wavelength. The extinction coefficient is the sum of an absorption coefficient α (λ,T) and a scattering coefficient s (λ). This relationship removes the restriction to gray materials and so is greatly to be preferred for real materials such as minerals and rocks. Clark's approach was to separate the effects of absorption and scattering and to assume they could be simply summed. He made measurements on gem quality minerals [Clark, 1957b] in order to obtain reasonable values for α at room temperature and used these to estimate the radiative conductivity, neglecting the scattering coefficient. The values he obtained are given in Table I. It is apparent from his admittedly approximate treatment that radiative transfer is important in the thermal conductivity of the earth's outer mantle and the interior of the moon as well.

Volcanism and thermal conductivity are competing mechanisms in preventing complete melting in a radioactively heated planet. The uncertainty in the numerical values of planetary thermal conductivity is very important in attempting to establish the volcanic history of a planetary body such as the moon.

TABLE I

RADIATIVE CONDUCTIVITY [From Clark, 1957b]

Values are given in cal/cm sec °C

MINERAL	Temperature °K			
	1000	1500	2000	2500
Olivine	0.071	0.206	0.346	0.483
Diopside	0.016	0.057	0.106	0.173
Pyrope	0.001	0.005	0.018	0.044
Almandine	0.001	0.004	0.010	0.051
Grossularite	0.011	0.046	0.109	0.097

With this in mind we have started an investigation of a number of factors that enter into the precise determination of radiative conductivity. We have felt that the most important topics to be investigated were:

1. The variation of the absorption and refractive index with temperature up to the neighborhood of the melting points of the relevant minerals,
2. Refinement of the rather coarse current methods for estimating the scattering coefficient,
3. An examination of the validity of treating the absorption and scattering coefficients as independent entities that may be simply summed in the radiative transfer relationship.

Finally, the results of these considerations have been utilized to modify the numerical values for the thermal conductivity expected in the lunar interior and earth's upper mantle.

II. RADIATIVE CONDUCTIVITY IN TERMS OF THE MACROSCOPIC PARAMETERS $\bar{n}$, K AND S

Since it is impossible to specify the spatial distribution of n and k in microscopic detail, the scattering must be regarded as a statistical process. Under these conditions the radiative conductivity must first be calculated in terms of the macroscopic parameters $\bar{n}$, K and S which are, respectively, the average refractive index, absorption coefficient, and backscattering coefficient of the medium for diffuse radiation. These three parameters must then be evaluated in terms of a suitable microscopic model of the medium which specifies the spatial variations of n and k.

An expression for the radiative conductivity can easily be derived by Schuster's [1905] two-flux method in which the diffuse radiation, per unit wavelength interval, crossing unit area of any horizontal plane is divided into an outgoing part I and an ingoing part J. The equations for the vertical variation of I and J are:

$$\frac{dI}{dz} = -(K + S)\, I + SJ + K\bar{n}^2 B \tag{3}$$

$$-\frac{dJ}{dz} = -(K + S)\, J + SI + K\bar{n}^2 B \tag{4}$$

where z is measured vertically upwards. Eq. (3) states that the upward-going flux in crossing a layer of medium of unit thickness, decreases by an amount (K + S) I owing to absorption and backscattering, increases by an amount SJ owing to backscattering of the downward-going flux, and increases by the amount $K\bar{n}^2 B$ owing to self-emission from the layer. In the emission term, B is the blackbody flux density per unit wavelength interval in a vacuum. The factor $\bar{n}^2$ allows for the increased flux density in a medium of average refractive index $\bar{n}$ that results from the reduced wavelength in the medium.

In the case of uniform temperature, for which I and J are equal and spatially uniform, Eq. (3) reduces to

$$I = \bar{n}^2 B \tag{5}$$

which is the correct expression for the flux density in a uniform temperature cavity of refractive index $\bar{n}$.

Under steady-state conditions the net flux I - J must be uniform. Thus

$$\frac{d}{dz} (I - J) = 0 \tag{6}$$

Thus, on adding (3) and (4), we find

$$I + J = 2 \bar{n}^2 B \tag{7}$$

Subtraction of (3) from (4) then gives

$$I - J = - \frac{1}{K + 2S} \frac{d}{dz} (I + J) = - \frac{2}{K + 2S} \frac{d}{dz} (\bar{n}^2 B) \tag{8}$$

The total net flux for all wavelengths is

$$\begin{aligned} q &= \int_0^\infty (I - J) \, d\lambda \\ &= - 2 \int_0^\infty \frac{1}{K + 2S} \frac{d}{dz} (\bar{n}^2 B) \, d\lambda \\ &= - 2 \frac{\partial T}{\partial z} \int_0^\infty \frac{1}{K + 2S} \frac{\partial (\bar{n}^2 B)}{\partial T} \, d\lambda \end{aligned} \tag{9}$$

The radiative conductivity is therefore

$$C_r = \frac{q}{- \frac{\partial T}{\partial z}} = 2 \int_0^\infty \frac{\frac{\partial (\bar{n}^2 B)}{\partial T} \, d\lambda}{K + 2S} \tag{10}$$

Comparison of our result (Eq. (10)) with the result of Clark (Eq. (2)) shows a number of differences:

1. The refractive index n appears inside the derivative with respect to temperature in Eq. (10). Apparently, Clark assumed that n was independent of T.

2. The factor in front of the integral differs. This is explained below.

3. The quantity $K + 2S$ in Eq. (10) is not necessarily the same as the absorption coefficient for collimated radiation in a homogeneous medium plus a scattering coefficient of a non-absorbing medium as Clark implies in his paper. Both K and S are, in general, complicated functions of the optical constants of the individual grains of the medium, of the grain size, and of the wavelength.

Evaluation of the integral in Eq. (10) requires that K and S be expressed in terms of the optical constants n and k and the geometry of the medium. To do this we will consider three models of increasing complexity.

In the first model the optical constants are spatially uniform. Thus there is no scattering and the only problem is to evaluate the diffuse absorption coefficient K in terms of the collimated beam absorption coefficient α. The simple result $K = 2\alpha$ is obtained.

The second model consists of alternating parallel layers with different optical constants. This model is mathematically tractable and demonstrates that the result $K = 2\alpha$ is still valid even when S is considerably different from zero. However, the model fails to give a realistic value of S since the contribution of refraction to backscattering is automatically excluded by the parallel layer geometry.

The third model consists of a medium composed of two minerals A and B in which interfaces between A and B are randomly distributed both spatially and in angle. Calculation of S shows that refraction in many cases gives the dominant contribution to the backscattering.

III. UNIFORM MODEL

When n and k are uniform the scattering coefficient S is zero. The diffuse absorption coefficient K can be calculated as follows. Figure 1 shows a typical ray of the diffuse radiation crossing a thin layer dz of the medium at an angle θ to the vertical. Since the distance traveled through the layer is $dz/\cos\theta$ a fraction

$$1 - e^{-\frac{\alpha dz}{\cos\theta}}$$

of the energy of the ray is absorbed in the layer. Here α is the parallel-beam absorption-coefficient given by

$$\alpha = \frac{4\pi k}{\lambda} \tag{11}$$

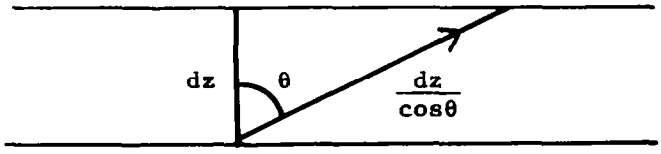

FIG. 1 TYPICAL RAY OF DIFFUSE RADIATION CROSSING A THIN LAYER

For diffuse radiation, the distribution in angle of the radiation passing upwards through unit area of the lower plane in Figure 1 is

$$di = \frac{1}{\pi} I \cos\theta \, d\omega \tag{12}$$

where I is, as before, the forward-going diffuse flux density and $d\omega$ is an element of solid angle. Thus the change in the diffuse flux due to absorption in dz is

$$dI = -\frac{1}{\pi} I \int_{\theta=0}^{\pi/2} \left(1 - e^{-\frac{\alpha dz}{\cos\theta}}\right) \cos\theta \, d\omega \tag{13}$$

Since dz is a differential quantity we can expand the exponential and neglect all higher order terms than the first. Thus

$$dI = -\frac{\alpha I dz}{\pi}\int_{\theta=0}^{\pi/2} d\omega = -2\,\alpha I dz \tag{14}$$

We can now compare Eq. (14) with the defining equation for the diffuse absorption coefficient K, which is:

$$\frac{dI}{dz} = -KI \tag{15}$$

Thus, for the uniform model,

$$\begin{aligned} K &= 2\alpha \\ S &= 0 \end{aligned} \tag{16}$$

The relation between K and α has been previously obtained by Kubelka [1948].

On substituting these values of K and S into Eq. (10), we get

$$C_r = \int_0^\infty \frac{1}{\alpha}\,\frac{\partial(n^2 B)}{\partial T}\,d\lambda \tag{17}$$

Eq. (17) differs slightly from the result of Czerny and Genzel [1952] and Eq. (2) in which a factor of 4/3 multiplies the integral (17). Czerny and Genzel calculated the radiative conductivity, not by the two-beam method of Schuster employed here, but by a direct integration of the emission from all points of the medium under the condition of an impressed temperature gradient. Their method, although much more complicated than the Schuster method, is undoubtedly correct. The question then arises as to the source of the discrepancy.

The difference can be traced to the assumption Eq. (12) that the fluxes I and J are completely diffuse and therefore have a cos θ distribution. This implies that the radiation in an element of volume has the angular distribution shown in Fig. 2a in which the radiation is isotropic in each

hemisphere but with a discontinuity at $\theta = 90°$. The correct distribution is shown in Fig. 2b in which the radiation in an element of volume is the sum of a uniform part and a part that varies continuously as cos θ from $\theta = 0$ to $\theta = 180°$.

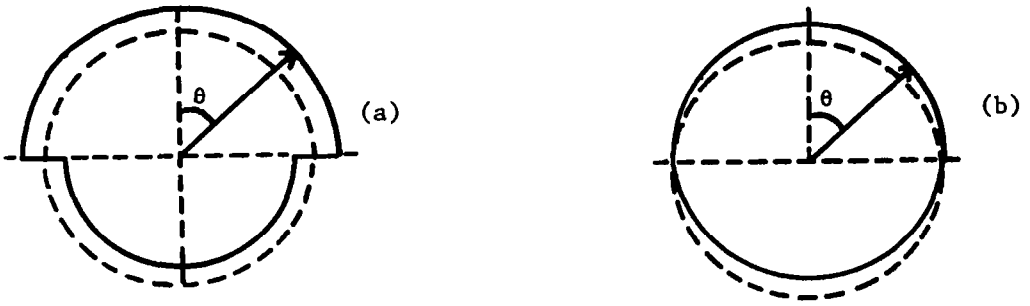

FIG. 2 ANGULAR DISTRIBUTION OF DIFFUSE RADIATION

The flux per unit area derived from the distribution of Fig. 2b has a cos θ part and a $\cos^2 \theta$ part. The correction to the absorption integral Eq. (13) which contains only a cos θ term, leads exactly to the required factor of 4/3 in Eq. (17).

The original Schuster theory, based on Fig. 2a, is simpler to apply than a theory based on Fig. 2b and is much more easily extended to include scattering. We will therefore base our further discussion on the pseudo-diffuse approximation of Fig. 2a.

IV. PARALLEL LAYER MODEL

In the parallel layer model the medium consists of horizontal alternating layers of minerals A and B. The A layers all have optical constants n_1, k_1 and thickness d_1. The B layers all have optical constants n_2, k_2 and thickness d_2. To calculate K and S for this medium we will compare the reflection and transmission coefficients of a "unit cell" of the medium of thickness $d_1 + d_2$ with the reflection and transmission coefficients of a slab of homogeneous medium that is characterized by the parameters K and S.

We choose the "unit cell," as shown in Fig. 3, in such a way that the reflection and transmission coefficients are the same for radiation incident on the bottom or the top of the cell. The cell consists of a layer of B between two half-thickness layers of A.

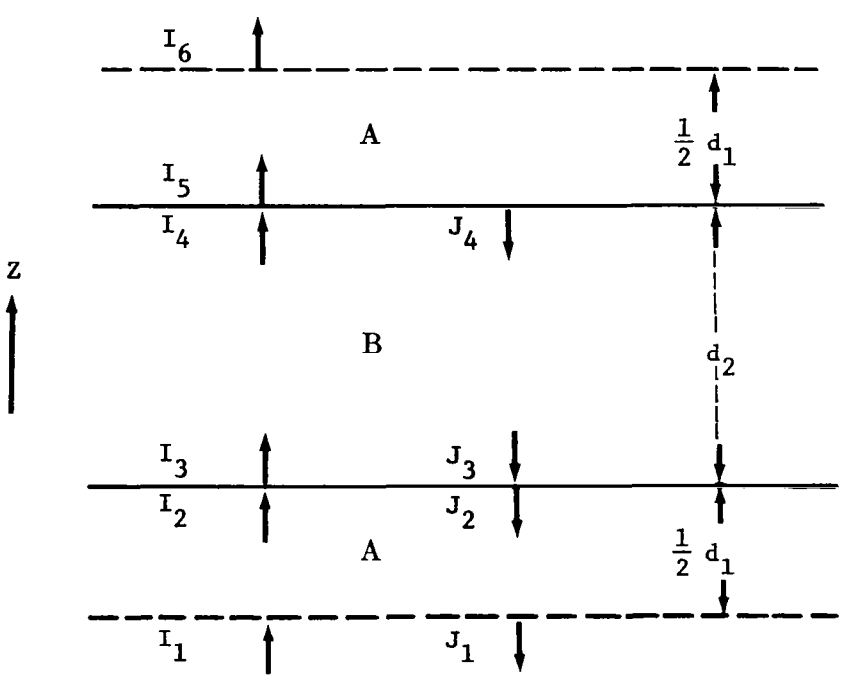

FIG. 3 LAYER MODEL UNIT CELL

Diffuse radiation I_1, incident from below, gives a reflected flux J_1 and a transmitted flux I_6. We wish to calculate the reflection coefficient $R = J_1/I_1$ and the transmission coefficient $T = I_6/I_1$.

Let r be the reflection coefficient at the interface between A and B. Then we can write two energy conservation conditions for each of the A-B interfaces in Fig. 3:

$$I_3 = (1 - r)\, I_2 + r\, J_3 \tag{18}$$

$$J_2 = (1 - r)\, J_3 + r\, I_2 \tag{19}$$

$$I_5 = (1 - r)\, I_4 \tag{20}$$

$$J_4 = r\, I_4 \tag{21}$$

Also, if 1/a and 1/b are the attenuation factors when the diffuse radiation travels distances $d_1/2$ and $d_2/2$ in A and B, respectively, then we have the following additional relations between the various fluxes shown

$$I_2 = I_1/a \tag{22}$$

$$J_1 = I_2/a \tag{23}$$

$$I_4 = I_3/b^2 \tag{24}$$

$$J_3 = J_4/b^2 \tag{25}$$

$$I_6 = I_5/a \tag{26}$$

The nine equations (18) - (26) can readily be solved for the ratios J_1/I_1 and I_6/I_1. The results are

$$R = \frac{J_1}{I_1} = \frac{r\,(b^4 + 1 - 2r)}{a^2\,(b^4 - r^2)} \tag{27}$$

$$\tau = \frac{I_6}{I_1} = \frac{b^2\,(1 - r)^2}{a^2\,(b^4 - r^2)} \tag{28}$$

Now, if α_1 and α_2 are the parallel-beam absorption coefficients in materials A and B, the diffuse absorption coefficients are $2\alpha_1$ and $2\alpha_2$, according to Eq. (14). Thus

$$a = e^{2\alpha_1 \frac{d_1}{2}} = e^{\alpha_1 d_1} = e^{\frac{4\pi k_1 d_1}{\lambda}} \tag{29}$$

$$b = e^{2\alpha_2 \frac{d_2}{2}} = e^{\alpha_2 d_2} = e^{\frac{4\pi k_2 d_2}{\lambda}} \tag{30}$$

Therefore Eq. (27) and (28) become

$$R = \frac{r\, e^{\frac{-8\pi k_1 d_1}{\lambda}} \left(e^{\frac{16\pi k_2 d_2}{\lambda}} + 1 - 2r \right)}{e^{\frac{16\pi k_2 d_2}{\lambda}} - r^2} \tag{31}$$

$$\tau = \frac{(1 - r)^2\, e^{\frac{8\pi}{\lambda}(k_2 d_2 - k_1 d_1)}}{e^{\frac{16\pi k_2 d_2}{\lambda}} - r^2} \tag{32}$$

We now have to derive the reflection and transmission coefficients of a slab of material, of thickness $d_1 + d_2$, characterized by the parameters K and S, as in Fig. 4. The differential equations for the fluxes I and J in the material are the same as Eqs. (3) and (4) without the self-emission terms:

$$\frac{dI}{dz} = -(K + S)\, I + SJ \tag{33}$$

$$-\frac{dJ}{dz} = -(K + S)\, J + SI \tag{34}$$

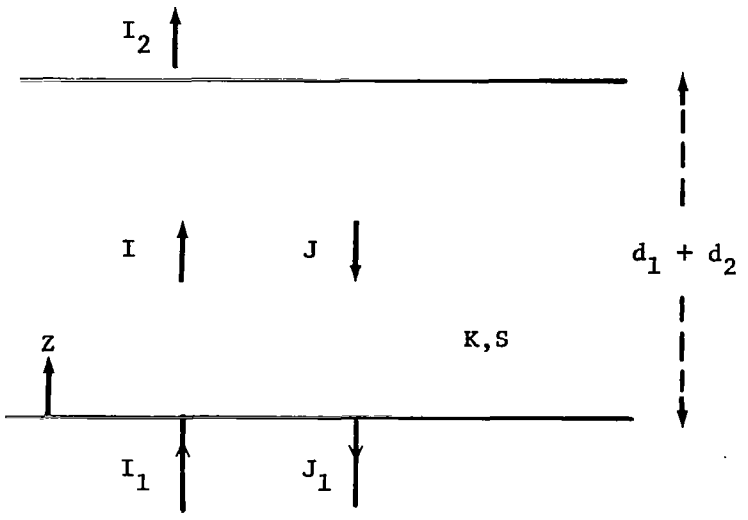

FIG. 4 HOMOGENEOUS MEDIUM EQUIVALENT TO THE LAYERED MEDIUM

The general solution of these equations is

$$I = A\, e^{\gamma z} + Be^{-\gamma z} \tag{35}$$

$$J = \left(\frac{\gamma + K + S}{S}\right) A\, e^{\gamma z} + \left(\frac{-\gamma + K + S}{S}\right) Be^{-\gamma z} \tag{36}$$

where

$$\gamma = \sqrt{K^2 + 2KS} \tag{37}$$

The boundary conditions are:

$$\left.\begin{aligned} I &= I_1 \\ J &= J_1 \end{aligned}\right\} \quad \text{at} \quad z = 0$$

$$\left.\begin{aligned} I &= I_2 \\ J &= 0 \end{aligned}\right\} \quad \text{at} \quad z = d_1 + d_2$$

These conditions give

$$A + B = I_1 \tag{38}$$

$$\left(\frac{\gamma + K + S}{S}\right) A + \left(\frac{-\gamma + K + S}{S}\right) B = J_1 \tag{39}$$

$$A\, e^{\gamma (d_1 + d_2)} + B\, e^{-\gamma (d_1 + d_2)} = I_2 \tag{40}$$

$$(\gamma + K + S)\, A\, e^{\gamma(d_1 + d_2)} + (-\gamma + K + S)\, B\, e^{-\gamma(d_1 + d_2)} = 0 \tag{41}$$

Algebraically one can solve Eqs.(38)- (41) for the ratios J_1/I_1 and I_2/I_1:

$$R = \frac{J_1}{I_1} = \frac{S \sinh \gamma (d_1+d_2)}{\gamma \cosh \gamma (d_1+d_2) + (K + S) \sinh \gamma (d_1+d_2)} \tag{42}$$

$$\tau = \frac{I_2}{I_1} = \frac{\gamma}{\gamma \cosh \gamma (d_1+d_2) + (K + S) \sinh \gamma (d_1+d_2)} \tag{43}$$

Finally, the equations for determining K and S are obtained by equating the reflection coefficients (31) and (42), and the transmission coefficients (32) and (43). The results are

$$\frac{S \sinh \gamma (d_1+d_2)}{\gamma \cosh \gamma (d_1+d_2) + (K+S) \sinh \gamma (d_1+d_2)} = \frac{r\, e^{\frac{8\pi k_1 d_1}{\lambda}} \left(e^{\frac{16\pi k_2 d_2}{\lambda}} + 1-2r \right)}{e^{\frac{16\pi k_2 d_2}{\lambda}} - r^2} \tag{44}$$

$$\frac{\gamma}{\gamma \cosh \gamma (d_1+d_2) + (K+S) \sinh \gamma (d_1+d_2)} = \frac{(1-r)^2\, e^{\frac{8\pi}{\lambda} (k_2 d_2 - k_1 d_1)}}{e^{\frac{16\pi k_2 d_2}{\lambda}} - r^2} \tag{45}$$

where $\gamma = \sqrt{K^2 + 2KS}$

It is to be noted that the righthand sides of Eqs. (44) and (45) are not symmetrical in k_1d_1 and k_2d_2. The reason for this is that in evaluating the reflection and transmission of a "unit cell" of the composite medium we assumed that the incident radiation started in medium A. If, instead, the radiation started in medium B, k_1d_1 and k_2d_2 in (44) and (45) would be interchanged. Therefore, to allow for the occurrence of both possibilities we must average the righthand sides with suitable weighting factors for the two cases before calculating K and S.

The interfacial reflection coefficient r is given, with sufficient accuracy, by the Fresnel formula at normal incidence:

$$r = \frac{(n_2 - n_1)^2 + (k_2 - k_1)^2}{(n_2 + n_1)^2 + (k_2 + k_1)^2} \tag{46}$$

as the reflectance of unpolarized radiation at angles of incidence out to moderately glancing angles is generally not very different from normal incidence reflectance.

The computer solution of the simultaneous Eqs. (44) and (45) for K and S for various combinations of n_1, k_1, d_1, n_2, k_2, d_2, and λ shows that K is always very close to $2\bar{\alpha}$, where $\bar{\alpha}$ is the average absorption coefficient no matter how much scattering there may be.

Thus, Eq. (10) becomes

$$C_r \approx \int_0^\infty \frac{\frac{\partial(\bar{n}^2_B)d\lambda}{\partial T}}{\bar{\alpha} + S} \tag{47}$$

V. COMPUTER SOLUTION

A computer program was written to solve Eqs. (44) and (45). Subroutines for independent solution of the righthand and lefthand sides of these equations were rapidly written and tested. However, it proved difficult to iterate the two equations to find the appropriate K and S for any set of optical parameters. While struggling with such convergence problems, we found a shortcut to solutions of these equations in a publication of S. Q. Duntley [1942]. In the paper, the author shows a plot using the lefthand side of Eq. (44) for the abscissa and the log of the reciprocal of the lefthand side of Eq. (45) for the ordinate with solutions in terms Kd and Sd shown as contours. In Fig. 5 we show this plot with the nomenclature changes to coincide with ours. Considerable insight into our problem was gained by using our computer program to find the values of the ordinate and abscissa on this plot and then reading values of K and S from it. Unfortunately, the range of the plot is limited and low values of K and S are difficult to estimate. Nevertheless, many answers could be obtained using this approach and in addition one source of some of our difficulties in the iteration can be seen. The contours of equivalent Kx and Sx go from essentially perpendicular intersection near the origin to nearly parallel geometry at the top of the figure. This can also be seen in Fig. 6 where we have plotted the solution contours for Eqs. (44) and (45) schematically using $\mu = (K^2 + 2KS)^{1/2}(d_1 + d_2)$ as the ordinate and $\eta = (K + S)\ (d_1 + d_2)$ as the abscissa. By comparing these two graphs, it is easily seen that essentially perpendicular intersection of the contours near the 45° line changes to essentially parallel contours in the lower part of the graphs.

Another problem that occurred in our computer solution for these equations is indicated by the 45° line. The area above this line is forbidden in that it represents negative values of S.

A subroutine was written in FORTRAN II to solve two simultaneous equations of the form $F_i(x_1, x_2) = 0$ using the Newton-Raphson method [Wegge, 1966]. This program starts with an initial estimate of x_1 and x_2 and makes use

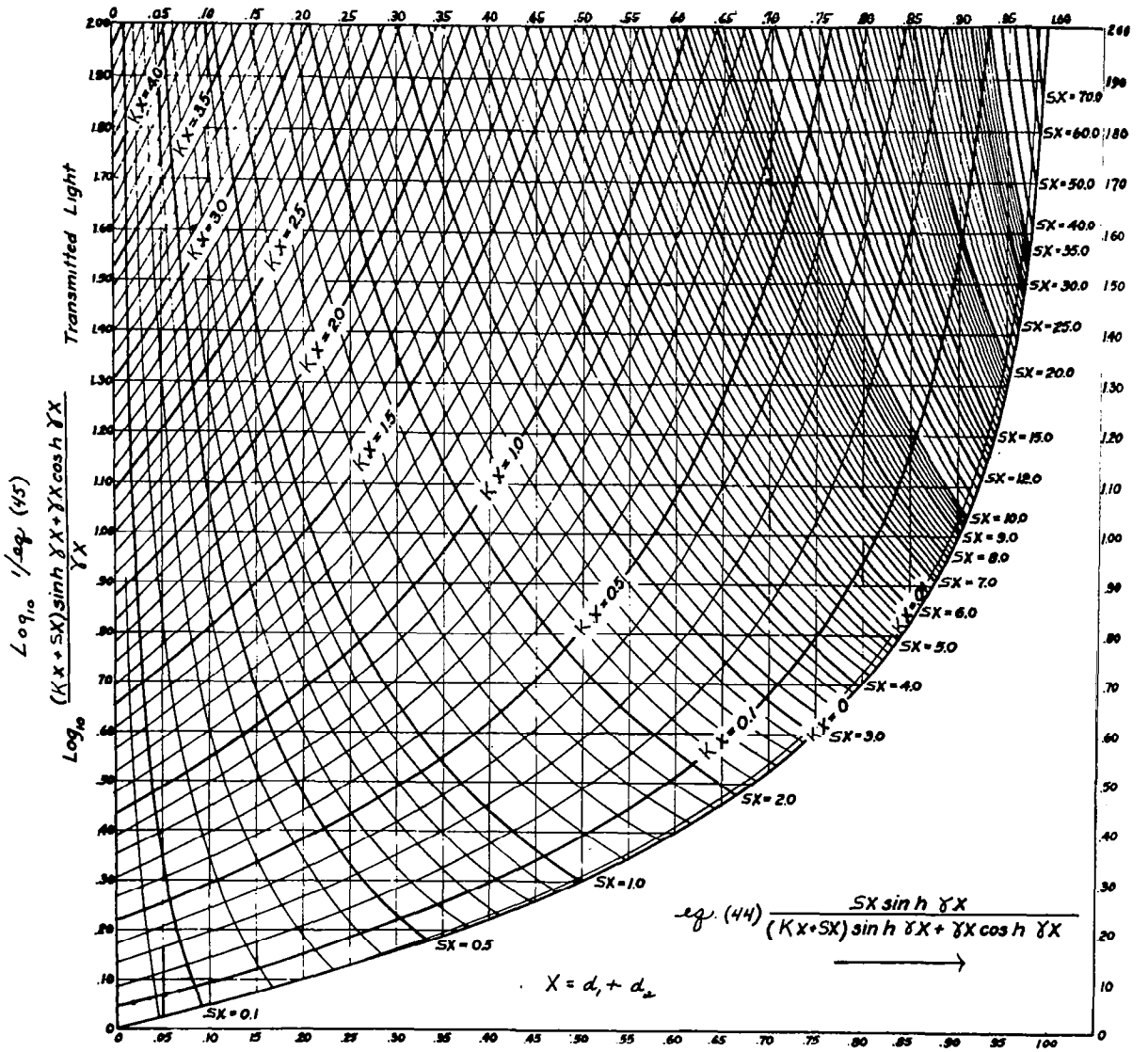

FIG. 5 SOLUTION CONTOURS FOR EQUATIONS 44 AND 45 (AFTER DUNTLEY)

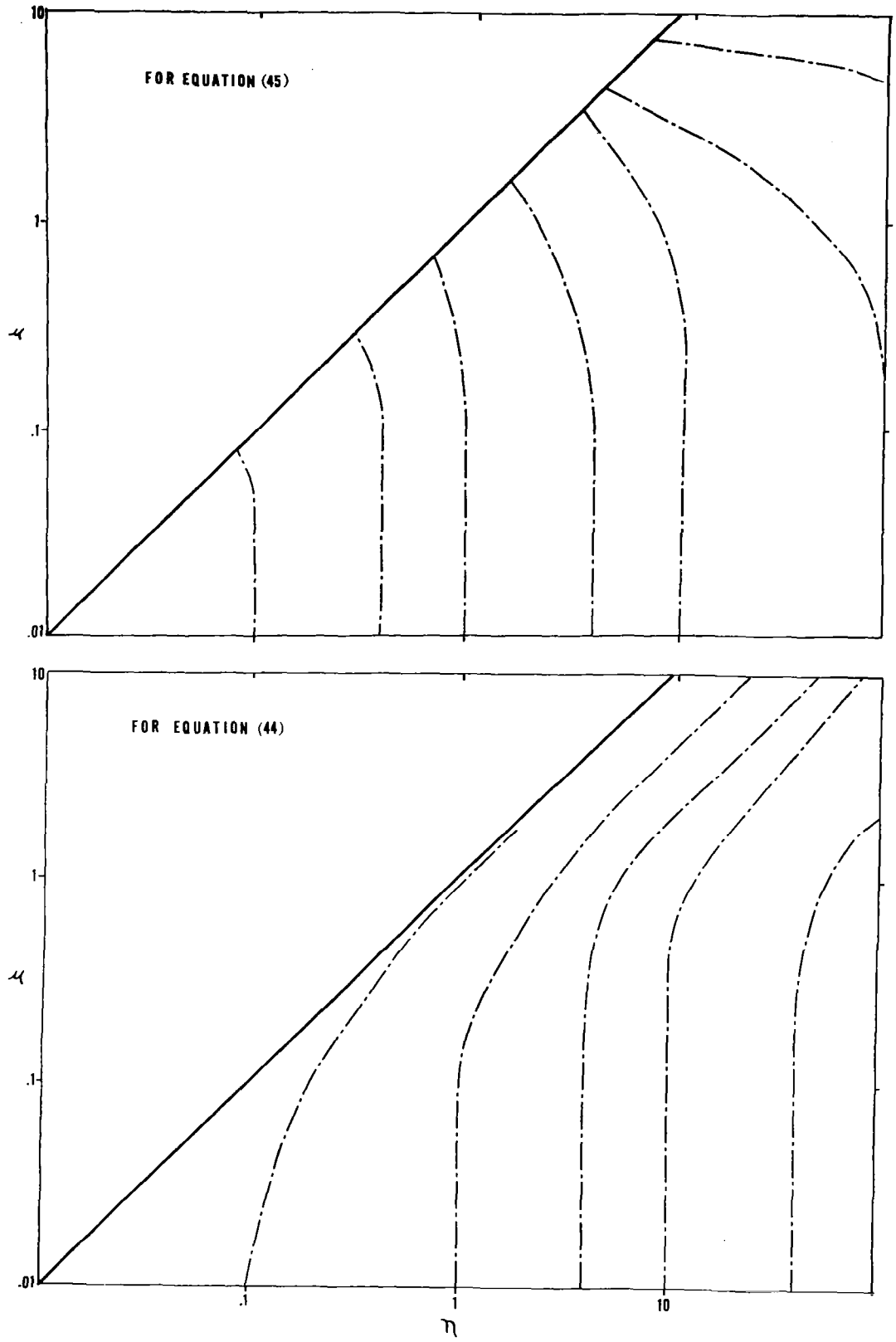

FIG. 6 SCHEMATIC SOLUTION CONTOURS USING μ AND η

of the iteration algorithm

$$x_i^{(n+1)} = x_i^{(n)} - \sum_{k=1}^{2} D_{ik}^{-1} F_k \left(x_1^{(n)}, x_2^{(n)}\right)$$

where D_{ik} is the Jacobian matrix whose i,j th element is

$$\partial F_i / \partial x_j \text{ evaluated at } \left(x_1^{(n)}, x_2^{(n)}\right)$$

to carry out a sequence of iterations until convergence is obtained. When combined with a subroutine for $D_{ik}(x_i)$ and $F_k(x_i)$ appropriate for Eqs. (44) and (45), this program was in most cases able to provide solutions.

The results of computer solution of Eqs. (44) and (45) are shown in Figs. 7, 8, and 9. At the time we carried out the computer solution to these equations, we had not allowed for the factor of 2 between the diffuse and collimated beam absorption coefficients discussed above. Therefore the exponents of the exponentials in the righthand sides of equations used in place of (44) and (45) were in error by a factor of 2. Except for the influence of k on R, the only correction necessary to the results was to consider the solutions K and S to be correct for values of k smaller by a factor of 2 than those actually used. The effect of k on R is completely negligible except where the refractive indices of the two media are essentially equal as the n's dominate the Fresnel reflection coefficients in all cases of moderately transparent media.

In Fig. 7 we have displayed the changes in K and S that result from varying the relative refractive index of the two materials at a number of constant values of kd/λ. As might be expected in the range of interest, K appears to depend very little on the refractive indices of the two media while S is insensitive to the absorption index k only at low values of k. S does go to zero when the refractive indices of the two media are equal, though it should be pointed out that the cases we have

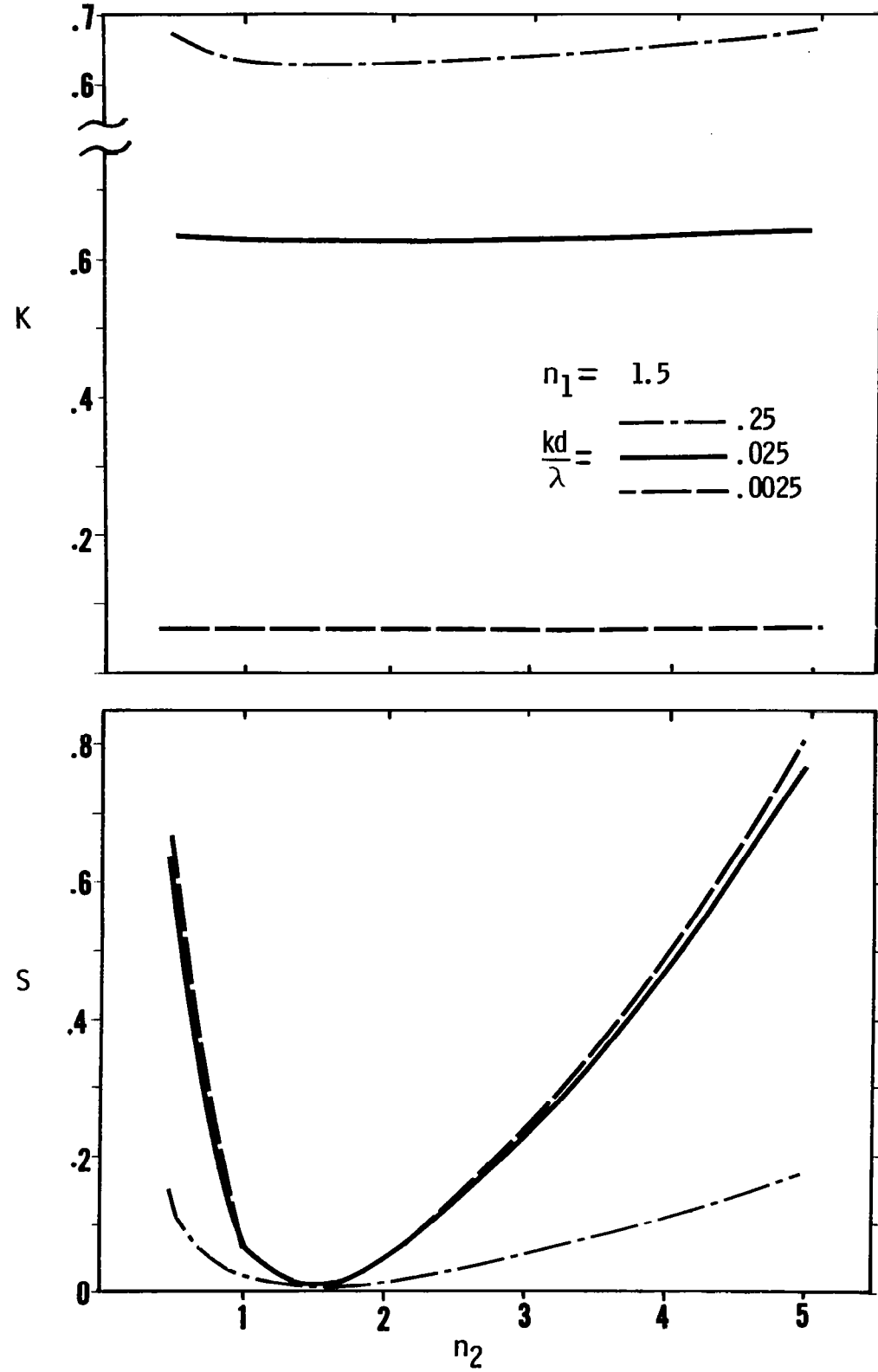

FIG. 7 COMPUTER RESULTS

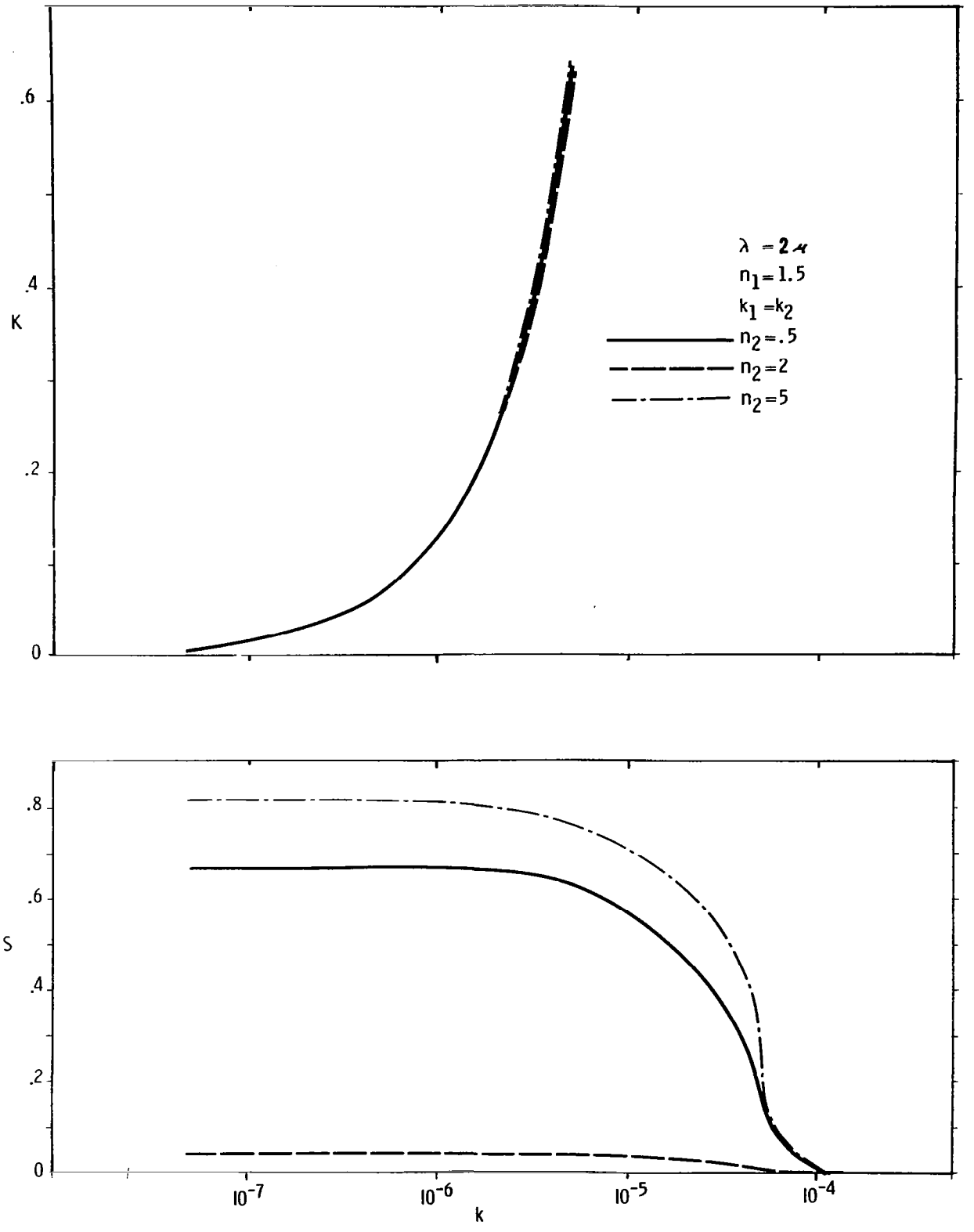

FIG. 8 COMPUTER RESULTS

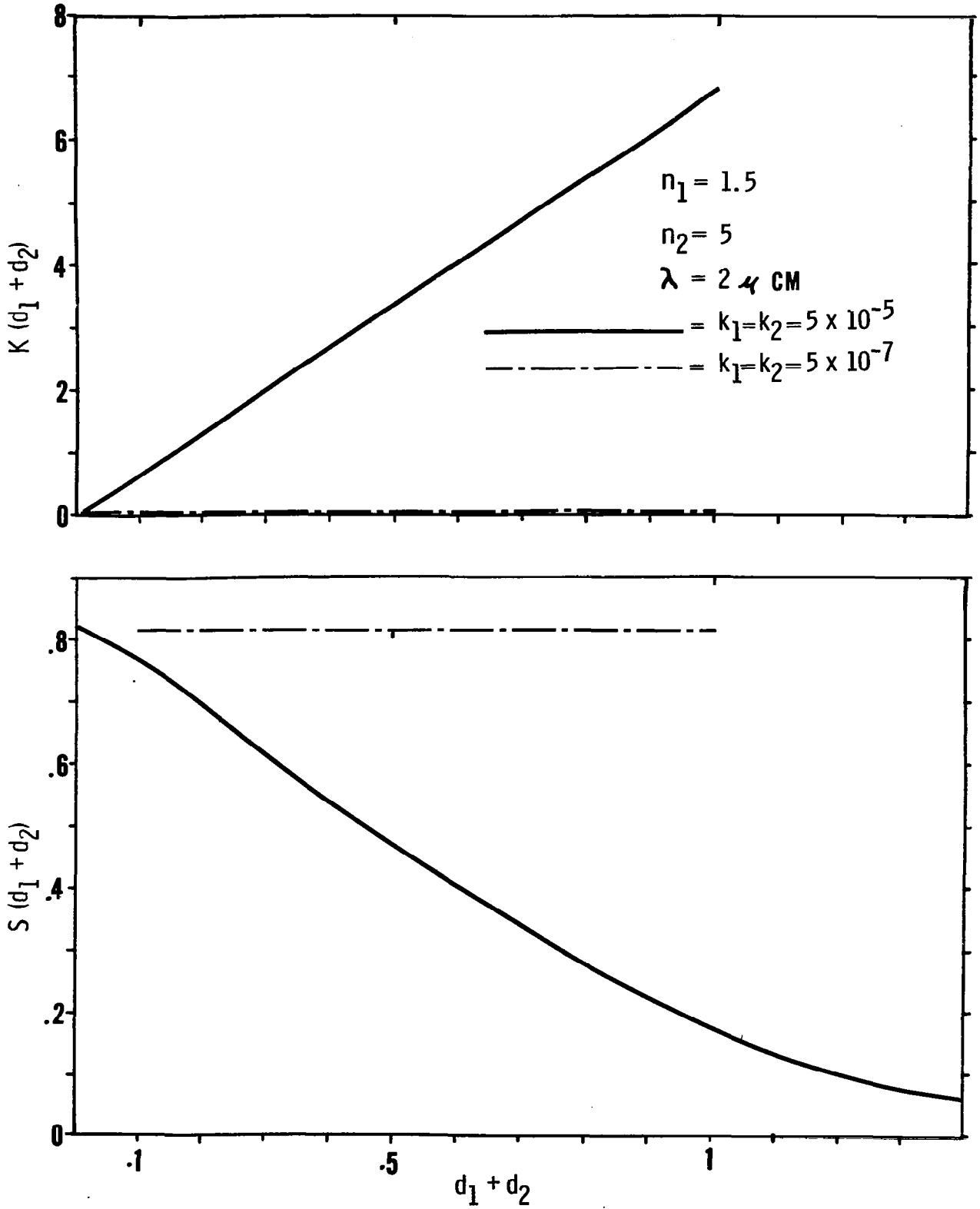

FIG. 9 COMPUTER RESULTS

run have involved small values of k compared to those for n in order to simulate expected values for minerals in the relevant spectral region. The k's on these figures are taken to be $\frac{k_1 + k_2}{2}$ and the d's are taken to be $d_1 + d_2$.

In Fig. 8, K and S are shown as functions of k for different values of the n's. The behavior of the scattering curve near $k = 10^{-4}$ is due to the fact that $\frac{kd}{\lambda}$ in the exponents of Eqs. (44) and (45) approaches unity in the calculations.

In Fig. 9, we show $K(d_1 + d_2)$ and $S(d_1 + d_2)$ plotted versus the layer thickness, $d_1 + d_2$. This scattering curve shows a drop in scattering coefficient with layer thickness which is to be expected for a Fresnel reflectance model as the number of scattering centers per unit length is decreased by increasing the path length.

Our results show that K is effectively equal to 2α for any value of K and S. It is easily seen that the development of our computer model enables us to obtain graphs for a great number of combinations of variations in the relevant parameters. It is, therefore, quite simple to explore the consequences of such a model. The program allows answers to be obtained in all but a very few cases of the input parameters (where an initial estimate of S equals zero). In general, the behavior of K and S with the various optical constants appears quite sensible to us. We feel that Clark's [1957a] use of α in Eq. (2) is justified. However, our calculation of S, using our Fresnel layer model, indicates a considerable dependence on α. The scattering estimate must therefore be made very carefully. As an example of this we made a calculation of the magnitude of S using similar values of the optical constants, characteristic sizes and volume fractions as those reported in Fig. 2.16-2 of our previous final report [McConnell et al., 1965]. For the case of a 0.1 cm radius, a discrepancy of approximately three orders of magnitude was discovered for the case of a very small refractive index difference between minerals. This large discrepancy was trace to two factors. First, the method of calculation previously used was based on an isolated scattering center treatment [Lee and Kingery, 1960] in which the total scattering coefficient was used in lieu of the back scattering

coefficient that is really applicable in radiative transfer. The factor relating these two coefficients is a function of opacity, relative refractive index and particle size. For the case under consideration here, this may be a large number. In addition, our layer model can only involve the Fresnel reflectance part of the back scattering. We are satisfied that neglect of the diffracted part of the back scattering is justified for the large particles under consideration but will show that in general there is a refractive term which is quite large for the particular optical constants that we are considering (see next section).

VI. RANDOM INTERFACE MODEL

In the random interface model we assume

1) that a straight line drawn in the medium in any direction randomly intersects interfaces between materials A and B, with an average number N of intersections per unit length, and

2) that the normal to each interface has a random direction uncorrelated with any other interface.

Fig. 10a shows a ray entering a thin horizontal layer of medium of thickness dz at a grazing angle β. The ray intersects an interface A-B at such an angle that backscattering by reflection occurs. In Fig. 10b, a ray intersects an interface C-D at such an angle that backscattering by refraction occurs. We wish to calculate the fraction of the diffuse radiation that is backscattered by each process. The fraction of the rays in a solid angle $d\omega$ at the angle β is $\sin\beta\, d\omega/\pi$. The chance that such a ray intersects an interface in traveling the slant distance $dz/\sin\beta$ is $N\, dz/\sin\beta$. The fraction of the rays in $d\omega$ that strike an interface is the product of the two expressions which is $N\, dz\, d\omega/\pi$. Per unit length in the z-direction the fraction is $N\, d\omega/\pi$.

Now let $f(\beta)$ be the fraction of interfaces that are favorably oriented to give backscattering by reflection and let $\overline{R}$ be the average reflection coefficient. Then the contribution of reflection to the backscattering coefficient is the product of $N\, d\omega/\pi$ and $f(\beta)$ and $\overline{R}$. Thus, the total contribution due to reflection is

$$S_{\text{reflection}} = \int \frac{N\, d\omega}{\pi} f(\beta)\, \overline{R} = \frac{N\overline{R}}{\pi} \int_{\beta=0}^{\pi/2} f(\beta)\, d\omega \qquad (48)$$

Likewise, if $g(\beta)$ is the fraction of the interfaces that are favorably oriented to produce backscattering by refraction, the total contribution due to refraction is

$$S_{\text{refraction}} = \frac{N(1 - \overline{R})}{\pi} \int_{\beta=0}^{\pi/2} g(\beta)\, d\omega \qquad (49)$$

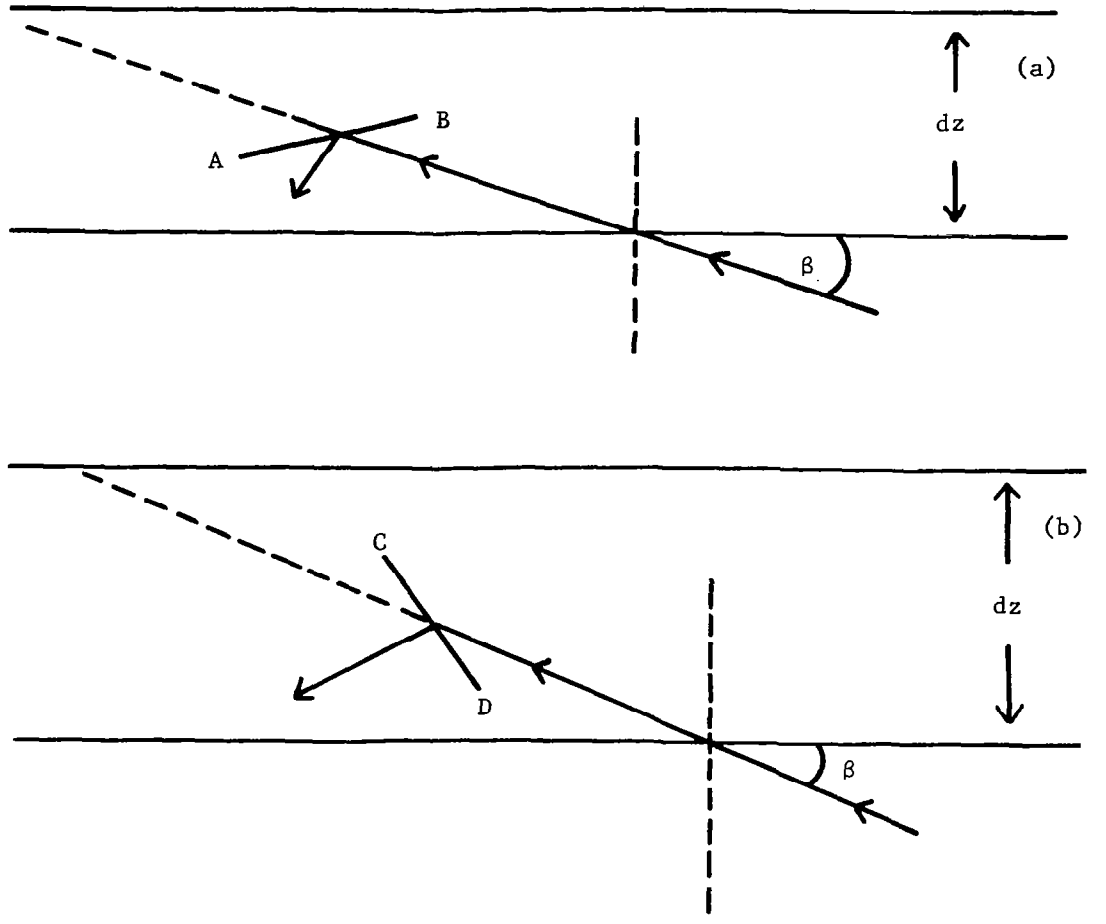

FIG. 10 SCHEMATIC DIAGRAM OF BACKSCATTERING BY REFLECTION AND REFRACTION

The backscattering coefficient is then

$$S = S_{\text{reflection}} + S_{\text{refraction}} \tag{50}$$

The function $f(\beta)$ is the fraction of all reflected rays that are backscattered. Since the interfaces are randomly oriented the reflected rays are uniformly distributed over all angles for any value of β. Thus, exactly one half of the rays are backscattered. Therefore

$$f(\beta) = \frac{1}{2} \tag{51}$$

Thus, from Eq. (48),

$$S_{\text{reflection}} = \frac{N \overline{R}}{2 \pi} \int_{\beta=0}^{\pi/2} d\omega = N \overline{R} \tag{52}$$

The calculation of $g(\beta)$ can be carried out with the help of Fig. 11 in which the large circle represents a unit sphere surrounding the point of incidence of the incident ray on an interface. The incident ray, when projected, intersects the sphere at the point P. The horizontal plane through the point of incidence intersects the sphere in the great-circle ACE. The line PC is part of a great circle, perpendicular to ACE, and is of length β. The spherical cap around P bounded by the small-circle BFD includes all possible refracted rays for all orientations of the interface. The size of the cap is defined by the angle χ of maximum deviation produced by refraction. This angle is given by

$$\cos \chi = \frac{n_1}{n_2} \tag{53}$$

where $n_1 < n_2$.

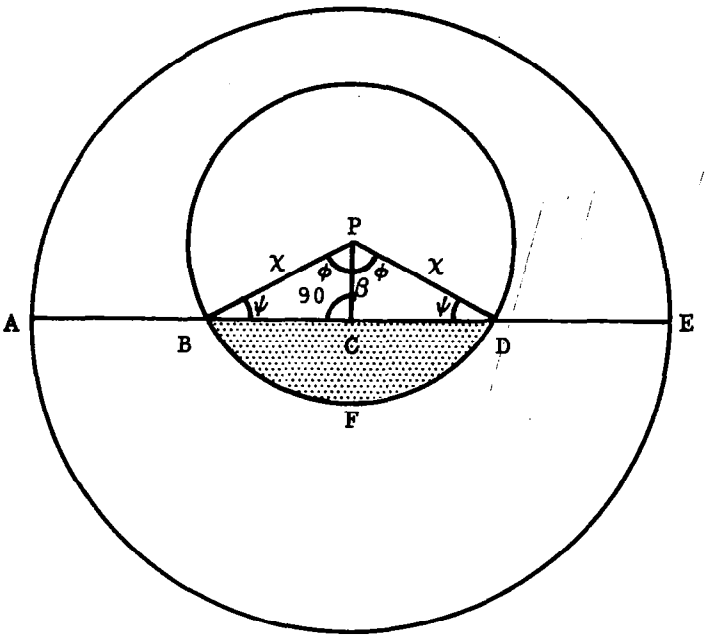

FIG. 11 UNIT SPHERE

The dotted area BFDCB includes all refracted rays that are backscattered. The function $g(\beta)$ is the ratio of this area to the area of the whole circular cap. The area of the cap is $2\pi\ (1 - \cos\chi)$. The area of the portion of the cap PBFD is $2\phi\ (1 - \cos\chi)$. The area of the spherical triangle PBCD is $2\phi + 2\Psi - \pi$. Thus the area of BFDCB which is the difference of PBFD and PBCD is $\pi - 2\phi \cos\chi - 2\Psi$.

Therefore

$$g(\beta) = \frac{\pi - 2\phi \cos\chi - 2\Psi}{2\pi\ (1 - \cos\chi)} \tag{54}$$

The angles ϕ and Ψ are indicated in Fig. 11. From spherical trigonometry:

$$\cos\phi = \frac{\tan\beta}{\tan\chi} \tag{55}$$

$$\sin\Psi = \frac{\sin\beta}{\sin\chi} \tag{56}$$

Thus Eq. (54) becomes

$$g(\beta) = \frac{\pi - 2 \cos \chi \cos^{-1}\left(\frac{\tan \beta}{\tan \chi}\right) - 2 \sin^{-1}\left(\frac{\sin \beta}{\sin \chi}\right)}{2\pi (1 - \cos \chi)} \tag{57}$$

We can now calculate $S_{refraction}$ from Eq. (49). The upper limit of the integral must be taken as χ since Fig. 11 shows that there is no back-scattering when $\beta > \chi$. On substituting for $g(\beta)$ from Eq. (57) and writing $2\pi \cos \beta d\beta$ for the element of solid angle $d\omega$, we get

$$S_{refraction} = \frac{N (1 - \bar{R})}{\pi (1 - \cos \chi)} \int_0^{\chi} \left\{ \pi - 2 \cos \chi \cos^{-1}\left(\frac{\tan \beta}{\tan \chi}\right) - 2 \sin^{-1}\left(\frac{\sin \beta}{\sin \chi}\right) \right\} \cos \beta d\beta \tag{58}$$

The three integrals can be integrated by standard methods to give:

$$\int_0^{\chi} \cos \beta d\beta = \sin \chi \tag{59}$$

$$\int_0^{\chi} \cos^{-1}\left(\frac{\tan \beta}{\tan \chi}\right) \cdot \cos \beta d\beta = \chi \tag{60}$$

$$\int_0^{\chi} \sin^{-1}\left(\frac{\sin \beta}{\sin \chi}\right) \cdot \cos \beta d\beta = \left(\frac{\pi}{2} - 1\right) \sin \chi \tag{61}$$

Thus

$$S_{refraction} = \frac{2 N (1 - \bar{R}) (\sin \chi - \chi \cos \chi)}{\pi (1 - \cos \chi)} \tag{62}$$

For small χ, Eq. (62) becomes

$$S_{refraction} \approx \frac{4}{3\pi} N (1 - \bar{R}) \chi \tag{63}$$

Fig. 12 shows the dependence of $S_{reflection}$ and $S_{refraction}$ on the refractive index ratio n_2/n_1, as calculated from Eqs. (52), (53), and (62). The ordinate is in units of N, the number of interfaces per unit length. The curve for refraction has a vertical tangent at $n_2/n_1 = 1$ while that for reflection has a zero slope. Thus refraction is the dominant mechanism for backscattering when n_2/n_1 is near 1.

As an example, let N = 10 interfaces per cm and $n_2/n_1 = 1.2$. Then $S_{reflection} = 0.1\ cm^{-1}$ and $S_{refraction} = 2.5\ cm^{-1}$.

The contribution of diffraction to backscattering is completely negligible compared with that of refraction. Since the linear dimensions of an interface are of the order of 1/N, the diffraction cone has an angle $\chi_{diffraction}$ given approximately by

$$\chi_{diffraction} = N \lambda \tag{64}$$

The cone angle for refraction is, from Eq. (53)

$$\chi_{diffraction} = \cos^{-1} \frac{n_1}{n_2} \tag{65}$$

Let $N = 10\ cm^{-1}$, $\lambda = 3\mu$ and $n_2/n_1 = 1.2$. Then $\chi_{diffraction} = 3 \times 10^{-3}$ radian and $\chi_{refraction} = 0.59$ radian.

This model disregards the effect on scattering of the absorption coefficient. Much of this effect is shown in the Fresnel layer model discussed above but the inordinately large refractive effect of the slant path rays would undoubtedly be reduced by absorption.

In conclusion, it seems apparent to us that assuming relatively large grain size, scattering is even less important than formerly thought [McConnell et al., 1965] [McConnell et al., 1957] [Clark, 1957a].

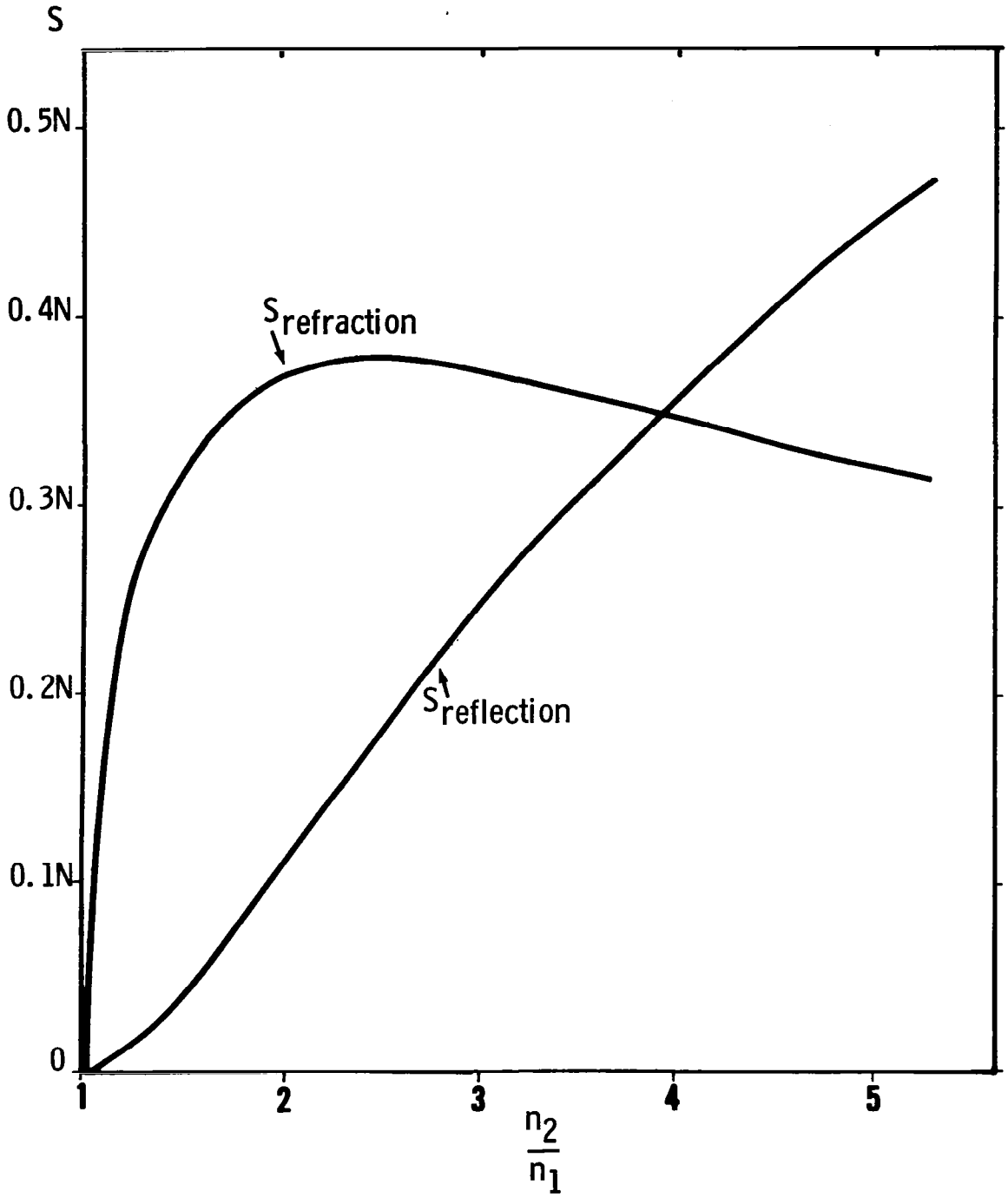

FIG. 12 BACKSCATTERING BY REFRACTION AND REFLECTION

VII. ABSORPTION COEFFICIENT AND MEAN FREE PATH

The important parameters in radiative transfer according to Eqs. (1), (2), and (10) and the expressions for ε, K and S are α, the absorption coefficient and n, the refractive index. Under conditions where scattering is small, the principal function to be evaluated is the magnitude of the spectral absorption coefficient $\alpha(\lambda,T)$ at the relevant temperatures and wavelengths.

As we are interested primarily in temperatures below the melting temperatures of olivine, blackbody considerations show that the most important spectral region for radiative transfer is the near infrared. For most rock-forming minerals this is a moderately transparent region, lying between the vibrational region of the infrared and the intrinsic "semiconductor" band gap region of the ultraviolet, although electronic absorptions such as those due to Fe^{++} [White and Keester, 1966] [Farrell and Newnham, 1965] occur in the region.

Although it is generally recognized that the absorption coefficient is temperature dependent, it has been customary in most calculations of the thermal history of planets to assume that it is constant [MacDonald, 1959]. On the assumption that the absorption spectrum is independent of temperature, Clark [1957b] was able to estimate the temperature dependence of the radiative conductivity for olivine, diopside, pyrope, almandine, and grossularite. His calculations utilize room temperature spectral data and thereby neglect any spectral changes that might occur at the relevant temperatures. Unfortunately, high temperature absorption coefficient and refractive index data in the relevant spectral region for minerals was not available. However, the small amount of experimental data on other materials which had been reported indicates that high temperature may have a drastic effect on absorption spectra in this region. In a study of the absorption coefficient and refractive index of Al_2O_3 up to 2300°K, Gryvnak and Burch [1965] observed a large increase in the absorption coefficient with increasing temperature, which was followed by a further large discontinuous increase on melting. The refractive index on the other hand only increased 0.05 up to 1970°K. Available data

on glasses [Grove and Jellyman, 1955] [Genzel, 1951] indicates a drop or very little change in absorption coefficient with increasing temperature to the vicinity of 1000-1400°C except for lead glass [Neuroth, 1952]. There appears to be an initial drop in absorption for all glasses and then an increase with increasing temperature. Some of the changes are irreversible, however.

In order to refine the estimates of the radiative conductivity we have begun a program of high temperature spectral measurements of likely mineral constituents of the mantle. The first minerals chosen for this program were peridot,diopside and oligoclase. These minerals were chosen for their relevance to our earlier work [McConnell et al., 1965] [McConnell et al., 1967] and their relative availability in reasonable size and clarity.

VIII. THE EXPERIMENTAL METHOD

There are in principle a number of ways of measuring the optical constants of materials. In general, two measurements must be made corresponding to the two parts of the complex refractive index

$$\tilde{n} = n - ik \tag{66}$$

although by use of the Kramers-Kronig relations one measurement at all frequencies may be substituted. The two experimental measurements can be either reflectance at two angles of incidence or polarizations, or transmittance using two sample thicknesses, or a combination of reflectance and transmittance.

The technique we have chosen is the combination measurement of normal incidence transmission and reflection. We have chosen this method in preference to the more common two thickness transmission measurement [for example, Gryvnak and Burch,1965], as mineral species are very difficult to duplicate exactly. The two thickness transmission method requires not only cancellation of identical reflection losses but identical absorption properties, as the measurement is, in essence, a determination of the absorption due to the excess path length in the thicker sample. For mineral species, therefore, the variation in absorption of two samples could be large enough to render the measurement one of sample variability rather than any inherent property of either sample.

It is sometimes the practice to correct a single transmission measurement:

$$\tau^* = \frac{(1 - r)^2 e^{-\alpha d}}{1 - r^2 e^{-2\alpha d}} \tag{67}$$

where τ^* is the apparent transmittance [McMahon, 1950] by disregarding the small effect of multiple reflections that is neglecting the denominator to give:

$$\tau^* = (1 - r)^2 e^{-\alpha d} \tag{68}$$

by using the normal incidence Fresnel relationship:

$$r = \frac{(n-1)^2 + k^2}{(n+1)^2 + k^2} \tag{69}$$

in simplified form when $k << n$

$$r = \frac{(n-1)^2}{(n+1)^2} \tag{70}$$

with handbook values of n or to assume that the highest apparent transmittance value corresponds to the reflectance losses. Both of these methods run into difficulties other than apparent in the explicit assumptions. The first neglects dispersion which can be significant near the beginning of an absorption region and the second does not allow for the possible effect of the wings of the remote absorption bands. Finally, the optical constants are functions of incident angle. For all these reasons we have chosen to measure transmission and reflection on the same sample at the same angle of incidence.

Our method is best suited to a non-scattering, perfectly parallel slab. Once again, real mineral samples of this type are exceedingly rare, and the alternative is to make hemispherical measurements. Such measurements are more difficult experimentally so we have spent considerable effort to obtain the least-scattering samples possible. An attempt is made to correct the measurements for the finite scattering that does occur in these samples. Fig. 13 shows a photograph of our samples as they appeared after grinding and optical polishing plane parallel faces. A brief description of the salient facts about these crystals is given in Table II.

It is important to make the observation that we are not a priori assuming the lunar interior or the earth's upper mantle to consist of such "flawless" stones. The need for optical clarity is an artifact of the measurement technique in that we are attempting to measure absorption phenomena in the absence of scattering for strictly experimental reasons. The data from our experiments are obtained as R^* and τ^*, the apparent

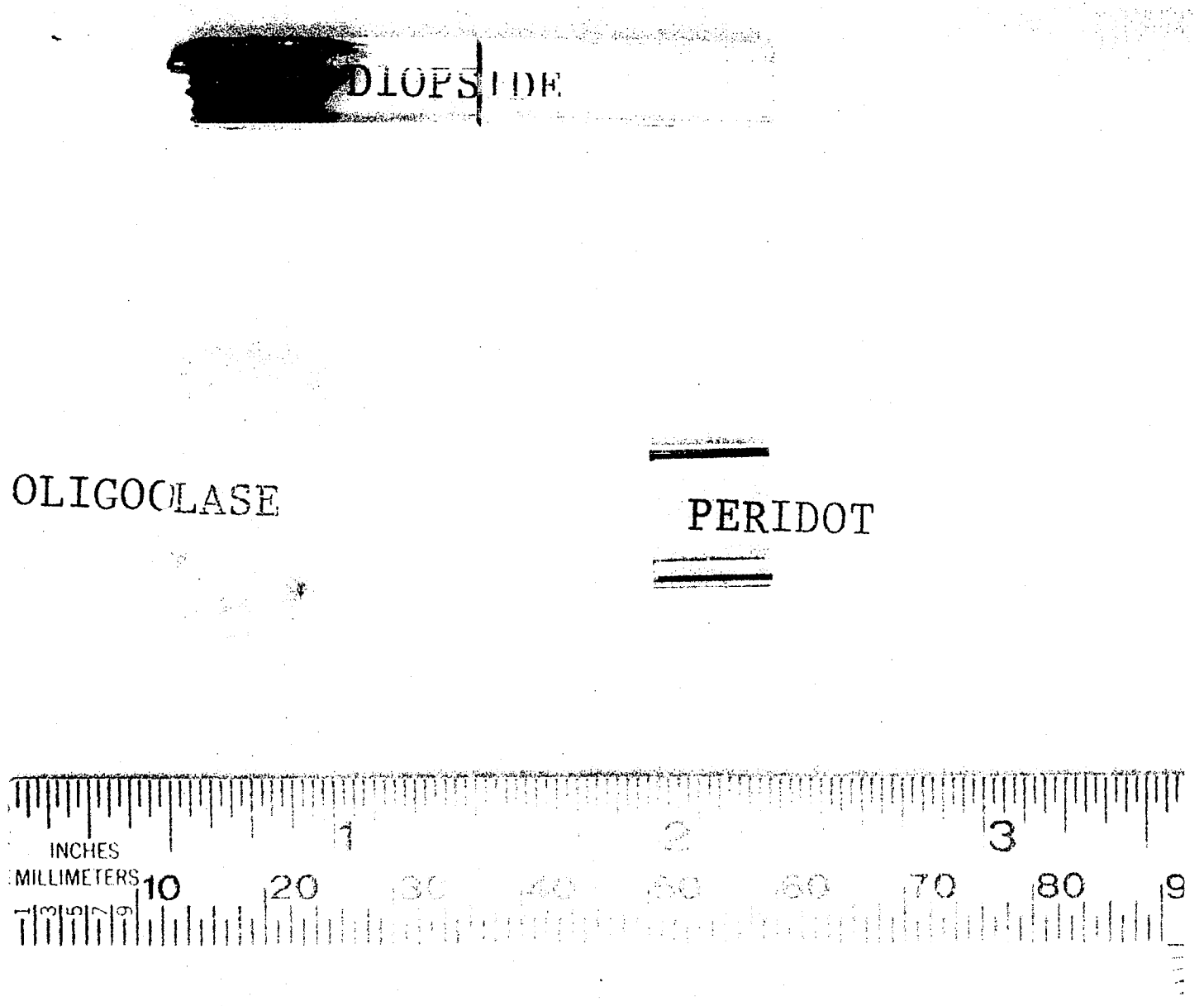

FIG. 13 MINERAL SAMPLES

reflectance and transmittance. These quantities involve the true reflectance and transmittance and the effects of multiple reflections. The apparent quantities can be reduced to the true quantities by computer techniques or simply by the use of the thermal radiation chart given by McMahon [1950] who developed this entire treatment.

This treatment essentially just combines Eq. (67) and a similar equation for apparent reflectance.

$$R^* = r\left[1 + \frac{(1-r)^2\, e^{-2\alpha d}}{1-r^2\, e^{-2\alpha d}}\right] \tag{71}$$

The true transmittance, τ and reflectance, r are then converted to the optical constants n and k by use of the Fresnel relationship (for normal incidence Eq.(69)) and the definition of transmittance, i.e.,

$$\tau = e^{-\alpha d} \tag{72}$$

where

$$\alpha = \frac{4\pi k}{\lambda} \tag{73}$$

TABLE II

CRYSTAL DATA

MINERAL	SOURCE	ORIENTATION STUDIED	THICKNESS
Corundum/Sapphire	The Linde Co. Synthetic	001	1.03 mm
Peridot	Wm.V.Schmidt Co.	3° off 100[b]	4.3 mm
Diopside	Harvard University[a] H88405 Rotenkopf, Tyrol	7-1/2° off 100[b]	3.48 mm
Oligoclase	Harvard University[a] Hawk Mine,Bakersville North Carolina	3° off 001[b]	6.77 mm

a. Courtesy of Professor C. Frondel.

b. Orientations obtained by X-ray techniques by Dr. Tony Marianno of the Kennecott Copper Ledgemont Laboratories.

IX. EXPERIMENTAL APPARATUS

Photographs of the experimental apparatus are shown in Figs. 14, 15, and 16. An optical diagram is given in Fig. 17. The apparatus was designed with a vertical tube furnace so that further measurements may be made on molten samples. It consists of two sets of fore optics, one for transmission measurements and one for reflection measurements. They are located below and above the vertically mounted tube furnace, respectively. Each assembly contains two source units, a globar and spherical mirror for the longer wavelengths and a tungsten ribbon lamp with a lens for the shorter wavelengths. A chopper is common to both sources. It is driven by a "Synchro" motor in synchonism with a camshaft of the phase sensitive demodulator at the output of the amplifier. A rotatable diagonal mirror on the transmission assembly and a similarly mounted aluminum coated calcium fluoride beamsplitter on the reflection assembly is turned to select either one of the two sources and directs a narrow cone of radiation into the tube furnace where it comes to a focus on the sample. This arrangement insures relative insensitivity of the transmitted or reflected beam to angular misalignment or wedge of the sample. The image of the sources on the sample is slightly larger than the intended sample area.

After leaving the sample (again via the beamsplitter in the reflection mode) the radiation is reflected by another diagonal and focused by a spherical mirror on the entrance slit of a Perkin Elmer model 98 single pass, single beam prism monochomator. This optical arrangement defines the active area of the sample as the slit image in the sample plane. A device to illuminate the slits from the inside of the monochromator has been provided so that this image and hence, the active area can be directly observed and therefore positioned properly. One must, of course, take care that the image of the source and the angle of its cone of illumination is always sufficient to fill the monochromator optic.

The monochromator is equipped with a high sensitivity (Charles Reeder,Inc.) thermocouple detector and a calcium fluoride prism, chosen for its good dispersion and transmission in our wavelength region and its insensitivity to normal handling and normal laboratory atmospheric conditions.

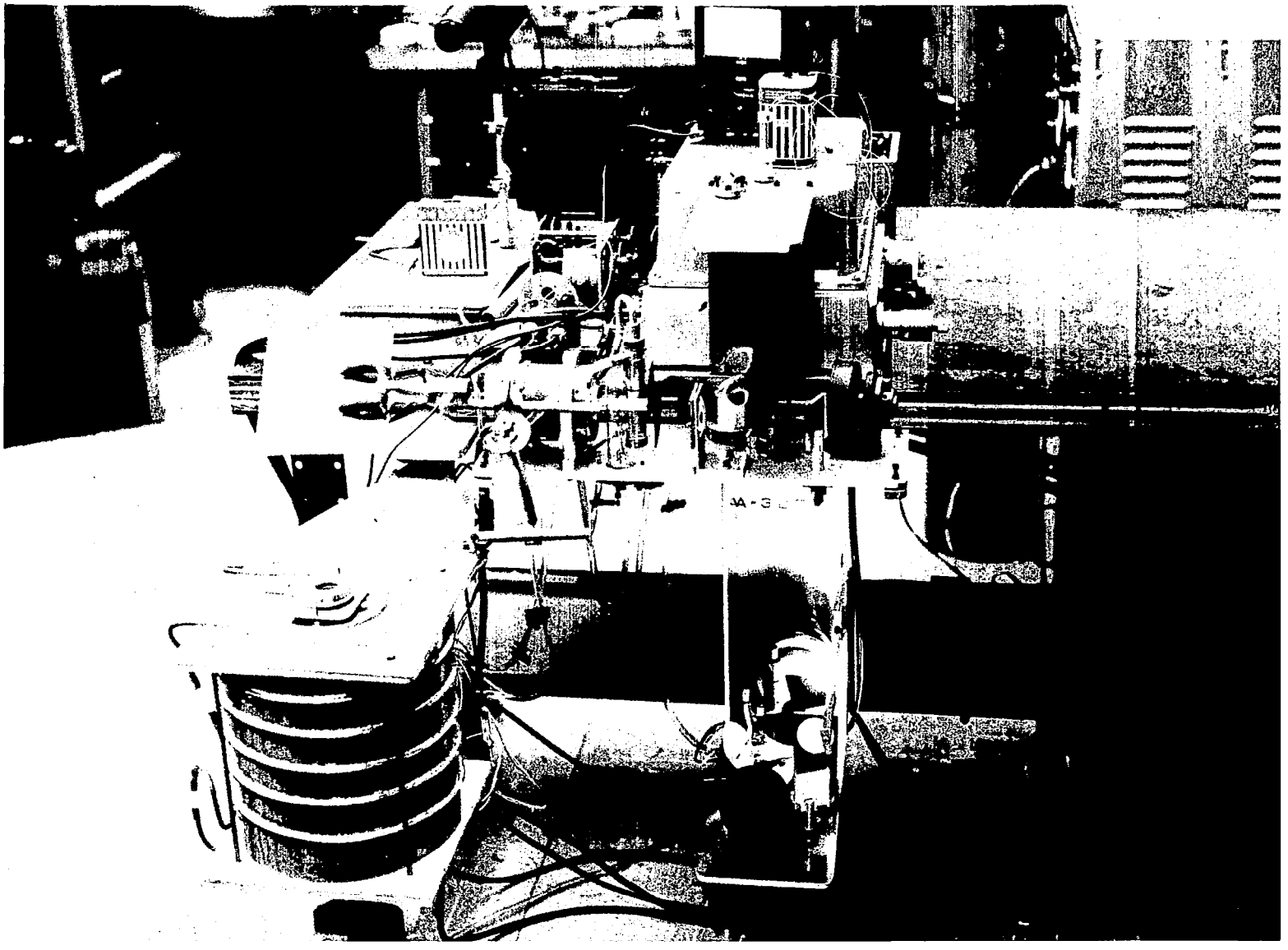

FIG. 14 EXPERIMENTAL APPARATUS

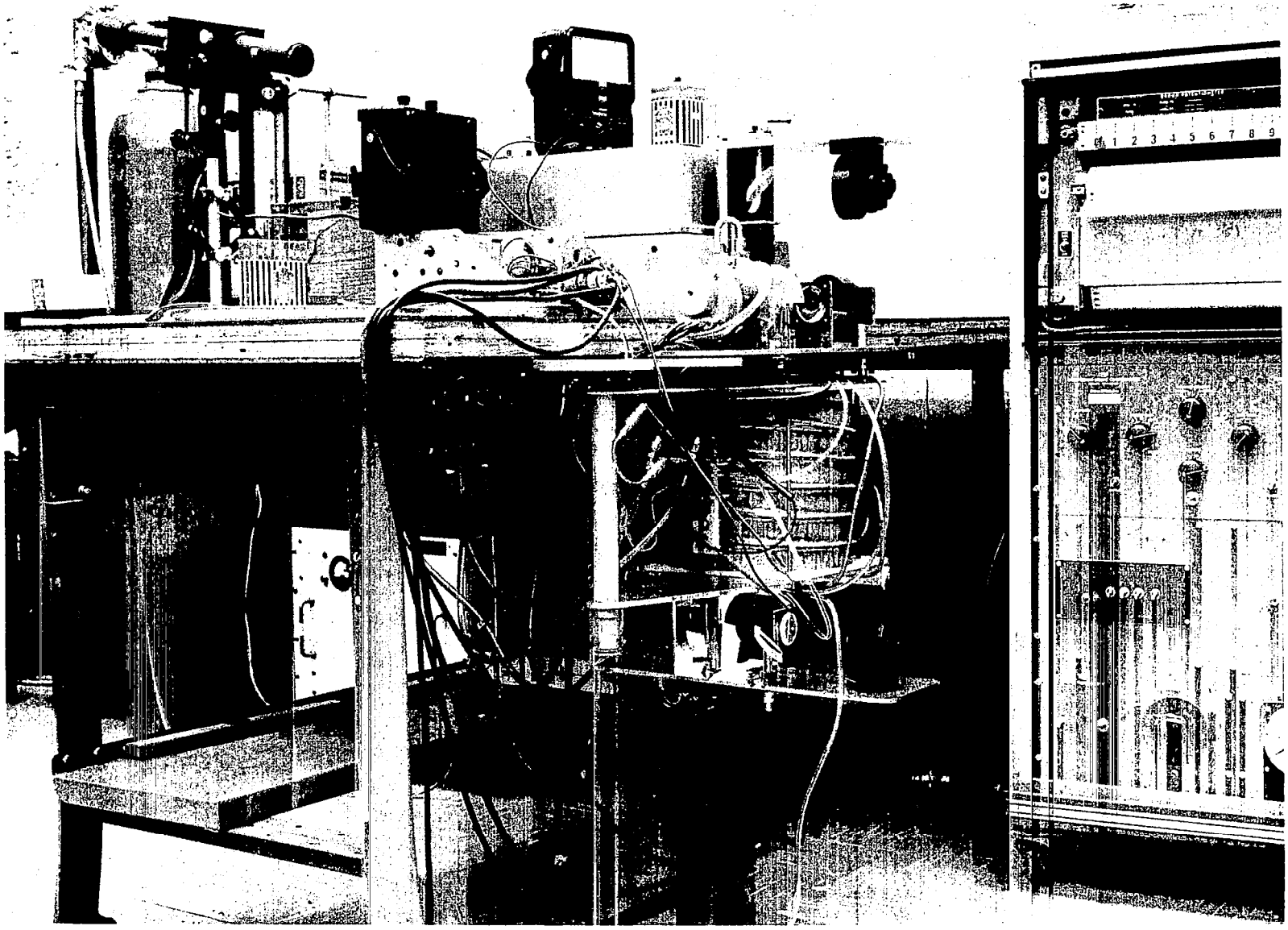

FIG. 15 EXPERIMENTAL APPARATUS WITH FURNACE IN PLACE

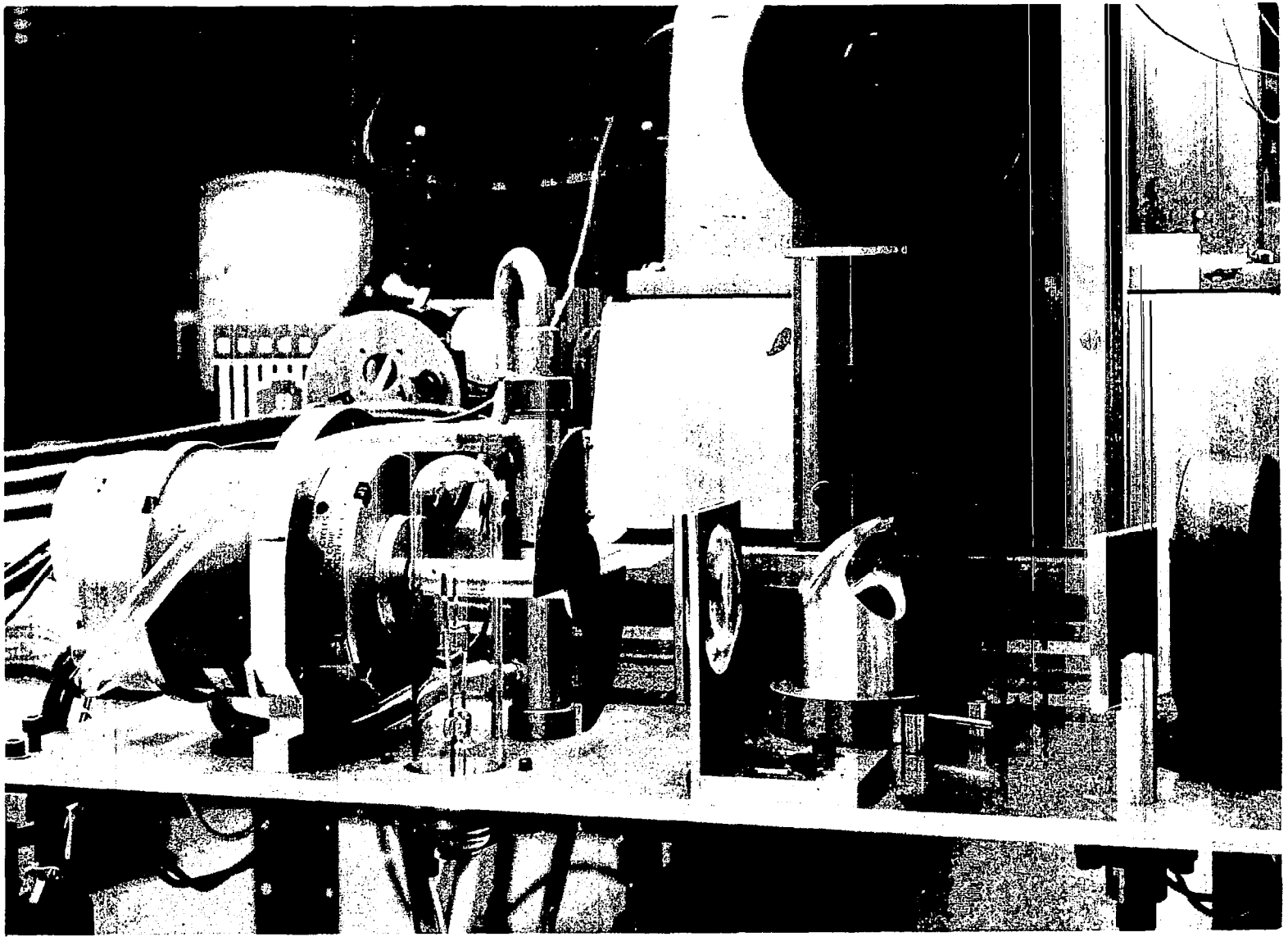

FIG. 16 REFLECTANCE SOURCE OPTICS

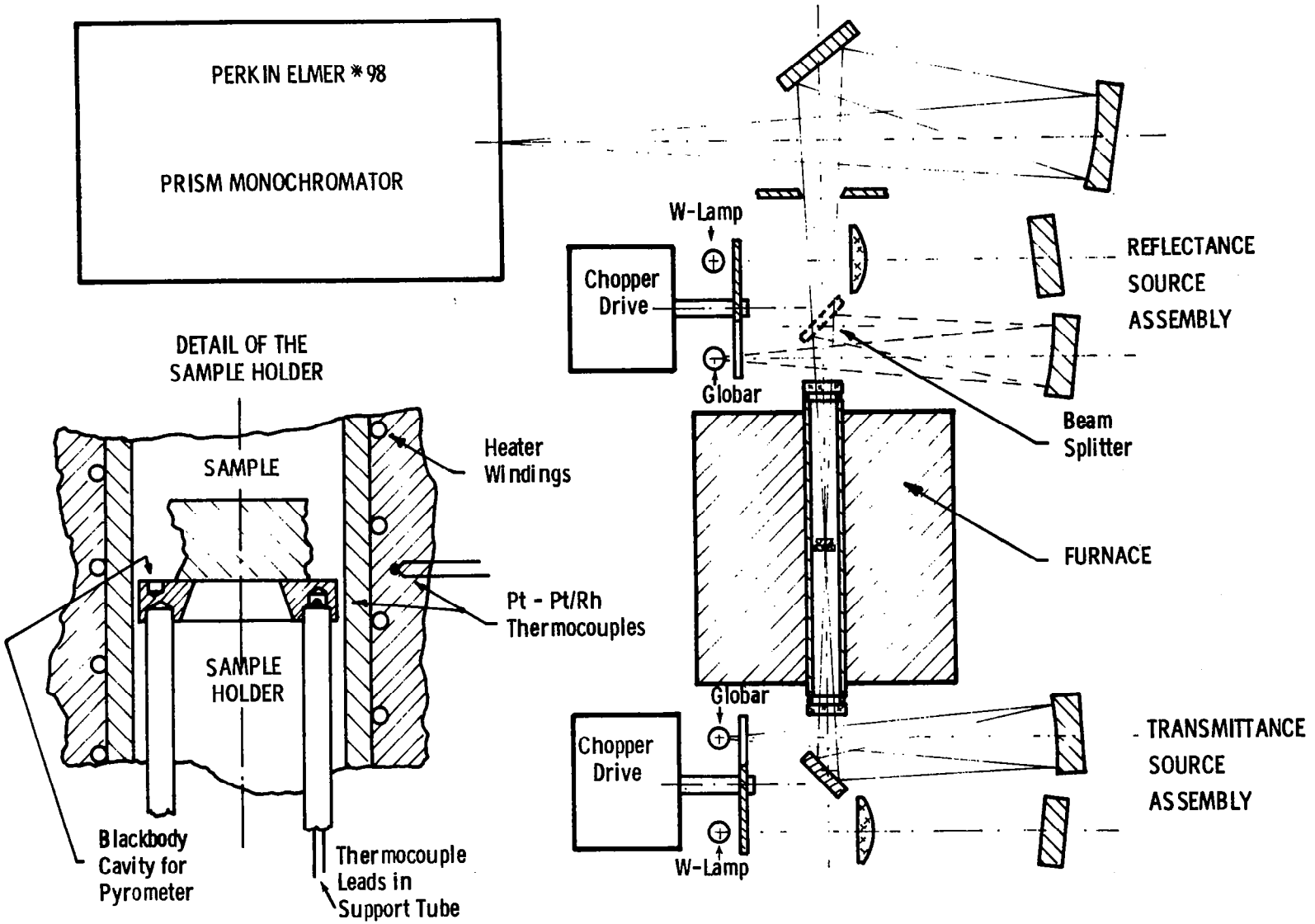

FIG. 17 OPTICAL DIAGRAM

The windows of the tube furnace, mounted in cooled windowholders, are also made of calcium fluoride. The furnace, while standard in principle, is made rather more solid and better insulated than normal. It is mounted on arms from a vertical shaft, so that it can be swung in and out of the optical path for ease of optical alignment of the sample and furnace. Cooling coils on all outside surfaces of the furnace carry away its maximum dissipation of almost 1 KW and thus avoid heating of the spectrometer and associated optics.

The furnace (see Fig. 17) consists of a 1 inch I.D. alumina tube having 3/16 inch thick walls and is 10-1/2 inches long. The center ca. 6-1/2 inches are wound with Kanthal wire. In order to reduce temperature gradients in the center portion of the tube, the tube is more densely wound toward the ends. The winding is covered with an alumina cement in which three thermocouples of Pt - Pt/Rh are imbedded. One thermocouple is located centrally and the other two are located an inch above and below the center, respectively. The thermocouples are electrically insulated from the heater wires by about 1/8 inch of alumina cement. The tube, with its heater and thermocouples is mounted in the end plates of a cylindrical furnace housing of about 10 inch diameter. The space between the tube and the shell is filled with insulation consisting of very fine alumina spheres.

At the very center of the tube is the sampleholder which stands on three alumina legs made of 1/8 inch diameter thermocouple tubing. One of the legs carried two 0.005 inch diameter Pt - Pt/Rh wires that are joined as a thermocouple inside the sample holder. As a further check on temperature, a small blind hole is provided in the top surface of the sampleholder, so that an optical pyrometer can be sighted through the top window of the furnace at this miniature "blackbody" cavity.

The entire arrangement was designed to enclose the sample as far as possible in an isothermal cavity, so that the sample temperature could be deduced accurately from the cavity temperature. The three outside thermocouples were intended to ascertain the gradient in the tube. The thermocouple in the sampleholder was designed to measure the temperature close to the sample and the radiation pyrometer would serve as a check on the sampleholder thermocouple.

In operation, the three outside thermocouples read values, as for instance: T (upper) = 780°C, T (center) = 1015°C, T (lower) = 875°C when the thermocouple inside the holder reads: T (holder) = 1040°C, and the pyrometer reads: T (pyrometer) = 1029°C.

These numbers which give a typical pattern show agreement better than needed for the purpose of the experiment. The low reading of the radiation pyrometer is due to reflection losses in the window and to some transparency of the sampleholder material at the wavelength of operation, i.e., at about 0.6 micron, which allows the pyrometer to partly sense the colder furnace end. The large difference between the upper and lower thermocouple readings is not understood. Simple calculations also show that the sample temperature must be very close to the tube temperature.

The power in watts radiated from the sample into each of the symmetrical hemispheres is given by:

$$P = \sigma \epsilon a T^4 \tag{74}$$

where ϵ is the sample emissivity and a is the sample area.

An equal amount is radiated back if the sample is in equilibrium inside a perfect cavity. If however the cavity has a small window (such as the windows of our furnace) to the relatively cold surroundings, the sample must be colder than the cavity in order to radiate no more power than it receives. In temperature equilibrium the relative difference in power would have been:

$$\frac{\Delta P}{P} \approx \frac{N \Delta \Omega a}{N \pi a} \tag{75}$$

where $\Delta \Omega$ is the solid angle subtended by the cold window. The radiance N in watts/sr cm in any direction from a radiator which follows Lambert's law is defined by:

$$\pi N = \sigma \epsilon T^4 \tag{76}$$

The relative temperature difference required to redress this imbalance is then:

$$\frac{\Delta T}{T} \approx \frac{\Delta P}{4P} \approx \frac{\Delta \Omega}{4\pi} \tag{77}$$

The solid angle of the cold window in this case is calculated to a first approximation from the tube's internal diameter and the length of the heated zone, measured from the center.

For an internal diameter of one inch and a length of three inches, we obtain $\Delta T/T \approx 0.7\%$ which approximates the experimental evidence. The small discrepancy is probably due to overestimating the tube emissivity at grazing angles.

We chose to make our measurements in an argon atmosphere in order to minimize thermal gradients at the sample and vaporization of the samples at high temperatures. The apparatus is run with a positive argon pressure to prevent atmospheric gases from entering the system. During early runs we discovered that an error due to tilting of the holder during the heating period was possible so an adjustment was provided. In order to minimize the dangers of cracking our specimens on heating, we have built a variac drive mechanism so that our samples can be heated slowly (73.5°C/hour) overnight to measuring temperatures. We heated spare samples of each of the minerals that we planned to run to high temperatures under argon in order to observe the type of problems that may be expected to occur. All samples withstood the temperatures involved although the "LAVA" (American Lava Corporation) sampleholders originally used cracked. We therefore had the high purity alumina holders machined for our actual runs. Some condensate of unknown origin has been found to form on our windows during the course of some runs.

A check of spectral purity was carried out by measuring the transmission of a National Bureau of Standards transmission filter between 0.6 and 2.4μ and comparing our measurements with values given by NBS (Fig. 18). We appear to be within 0.5% of their values over most of the curve, departing from their results by at most 3% in limited wavelength regions near 0.7 and 1.8μ. Spectral purity was also checked by means of a transmission run on a 2 mm sample of germanium. The results are shown in Fig. 18. The results of our mineral studies (vide infra) show our crystals to become almost opaque near 4.5μ. This indicates a lack of significant stray short wavelength radiation in the long wavelength regions.

The reference background used for the reflection measurements is a vapor deposited gold film (ca. 3000 Å thick) on a 2 mm sapphire disc. The reflectance of this standard is taken from Bennett and Ashley [1965].

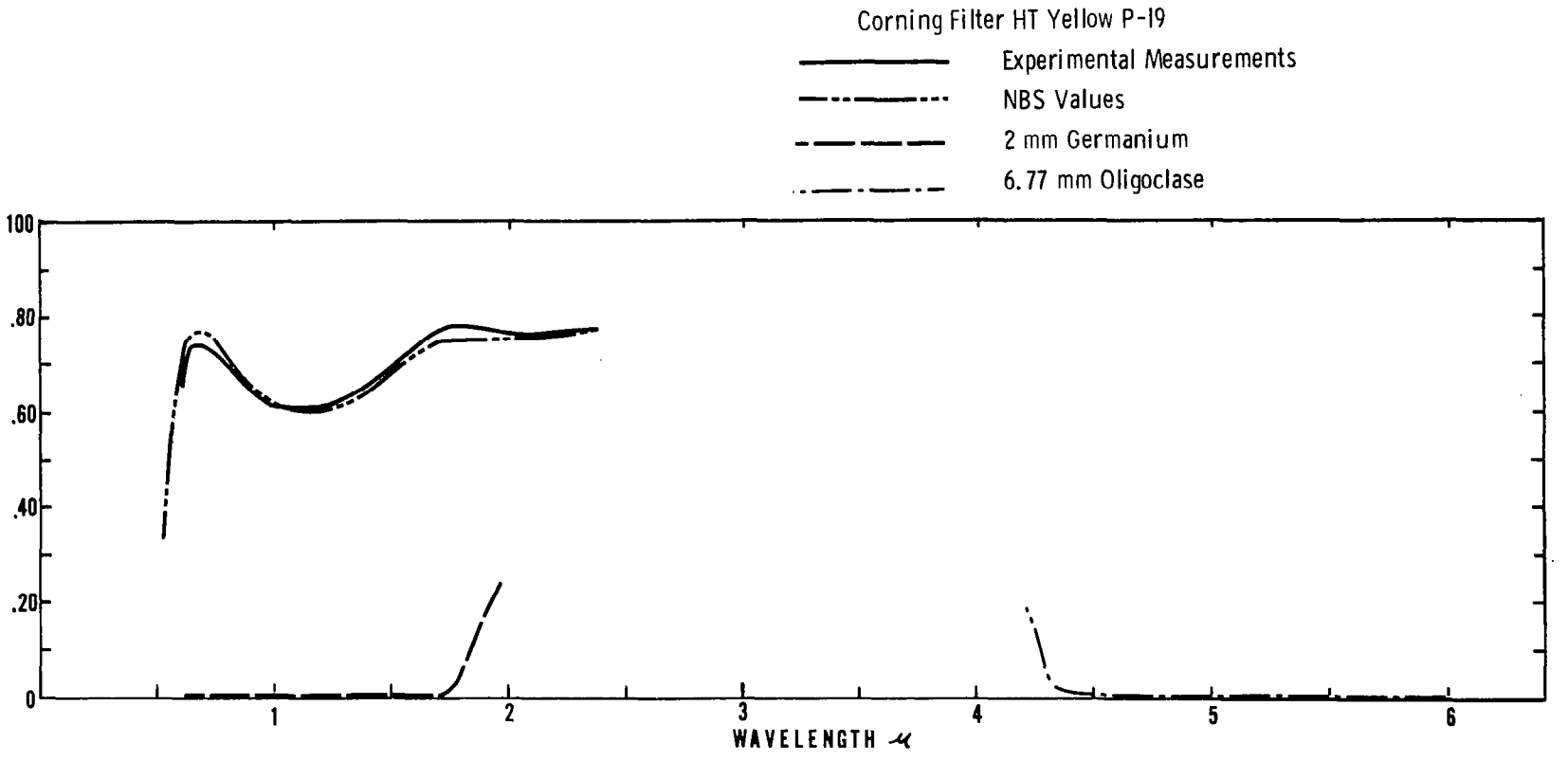

FIG. 18 SPECTRAL PURITY DATA

X. CRYSTAL SAMPLES

The pertinent data for the various samples used is shown in Table II. The best samples we were able to obtain were a clear crystal of oligoclase (approximate dimensions, 10 mm x 15 mm x 20 mm) as well as a long (approximate dimensions, 58 mm x 7 mm x 5 mm) clear diopside crystal from Professor Frondel of Harvard University, and a peridot gem stone obtained from Wm. V. Schmidt Co., Inc., a New York jeweler. Its approximate dimensions were 13 mm x 11 mm 6 mm. These samples were cut to suitable shapes and optically polished for our measurements. The crystals were cut to take advantage of the largest cross-sections available and for each crystal a second cut was made at a known crystal orientation. The light green peridot has a working cross-section of ca. 9 mm x 6 mm and a thickness of 4.3 mm. Some small inclusions are visible. The second cut was made perpendicular to the b axis and a 9 mm thickness was obtained. The cross-section is somewhat greater than 4 mm x 6 mm. The diopside sample was cut into three sections. It has a green area at one end that changes rather abruptly to a clear colorless crystal. The polishing revealed a series of cracks running lengthwise in the colorless part of this crystal (see Fig. 13). Measurements were made on the colorless ca. 21 mm x 6 mm sample (thickness 3.48 mm). Approximately half of one crystal is green but the color is somewhat variable. Measurements were also made on the green portion of this crystal and the results used in correcting for the scattering behavior on the colorless sample. The oligoclase sample has a cross-section of ca. 15 mm x 11.5 mm (thickness 6.77 mm). The second cut was made perpendicular to the apparent c axis (cross-section 12 mm x 7.5 mm and thickness ca. 11 mm). This sample on polishing shows a large number of small bubbles similar to those described by Smith [1963] (see Fig. 19). We planned to estimate the room temperature bubble scattering by making measurements below and above the temperature at which the bubbles disappear (loc cit) but as serious cracks occurred during heating we decided to proceed to the highest temperature immediately instead. The crystal orientations for all samples were obtained thanks to the efforts of Dr. Tony Marianno of the Kennecott Copper Laboratories. The peridot face we are measuring is 3° off the 100 face. The oligoclase data is for a face 3° off the 001 face and the diopside data is for a face 7-1/2° off the 100 face.

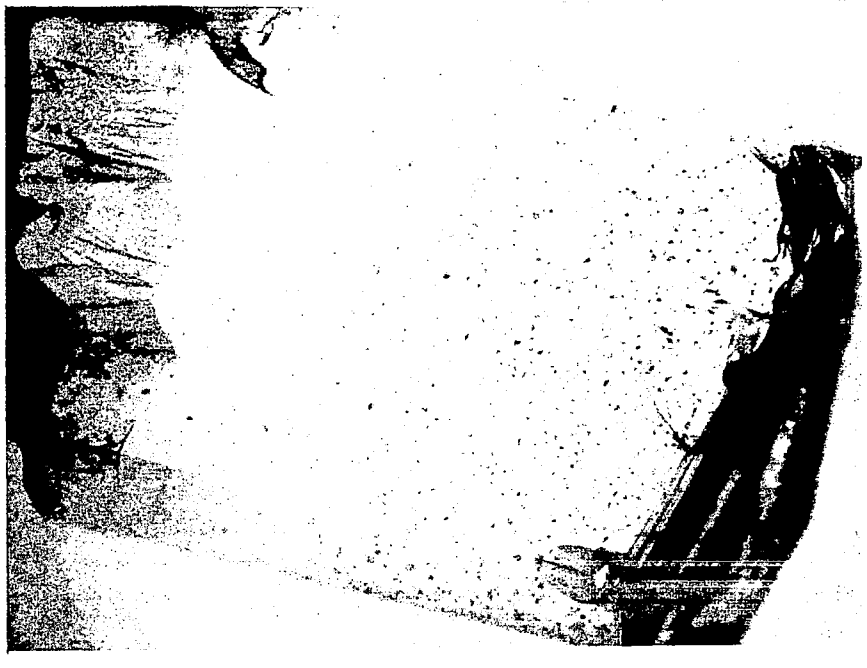

FIG. 19 OLIGOCLASE SAMPLE

XI. EXPERIMENTAL RESULTS

Sapphire

The spectroscopic apparatus was first used on 1.03 mm z-cut sapphire. This was done in order to ascertain the overall performance of the apparatus by comparing our results with those of other workers. Experimental difficulties were shown up by this means prior to obtaining the results shown below.

The apparent transmittance and reflectance of sapphire are shown in Fig. 20. The effect of heating to 1203°C is apparent in the broadening of the long wavelength absorption band. The data in Fig. 20 is in reasonable agreement with that given by Gryvnak and Burch [1965], except in the very transparent region near 2μ. The data in this region shows a T* and R* value greater than 1 which indicates an experimental error. In such a transparent region, such data cannot be converted to optical constants.

Peridot

The first silicate mineral that we ran was a green peridot gem stone. The room temperature spectrum is shown in Fig. 21. This spectrum is quite similar to data shown by Clark [1957b]. The apparent rise in reflectance at those wavelengths for which transmittance is a maximum is easily understood in terms of the greater amount of energy passing through the crystal, as compared to absorbing regions, and hence available to be reflected from the back face.

The strong absorption band centered at about 1.1μ has often been cited as the cause of the green color of many common silicates and ascribed to the presence of ferrous iron [White and Keester, 1966] [Farrell and Newnham, 1965]. It is presumed due to a $^5T_{2g} \rightarrow {}^5E_g$ electronic transition of Fe^{++} in octahedral coordination. The high frequency wing of the transition is thought to attenuate the red wavelengths resulting in a green color in transmission. Shankland [1966] has criticized this simple explanation of the color in olivines and posed a different interpretation. The most important points he makes are that the color is due mainly to a small number of impurity atoms at low symmetry interstitial or certain specific Mg^{++}

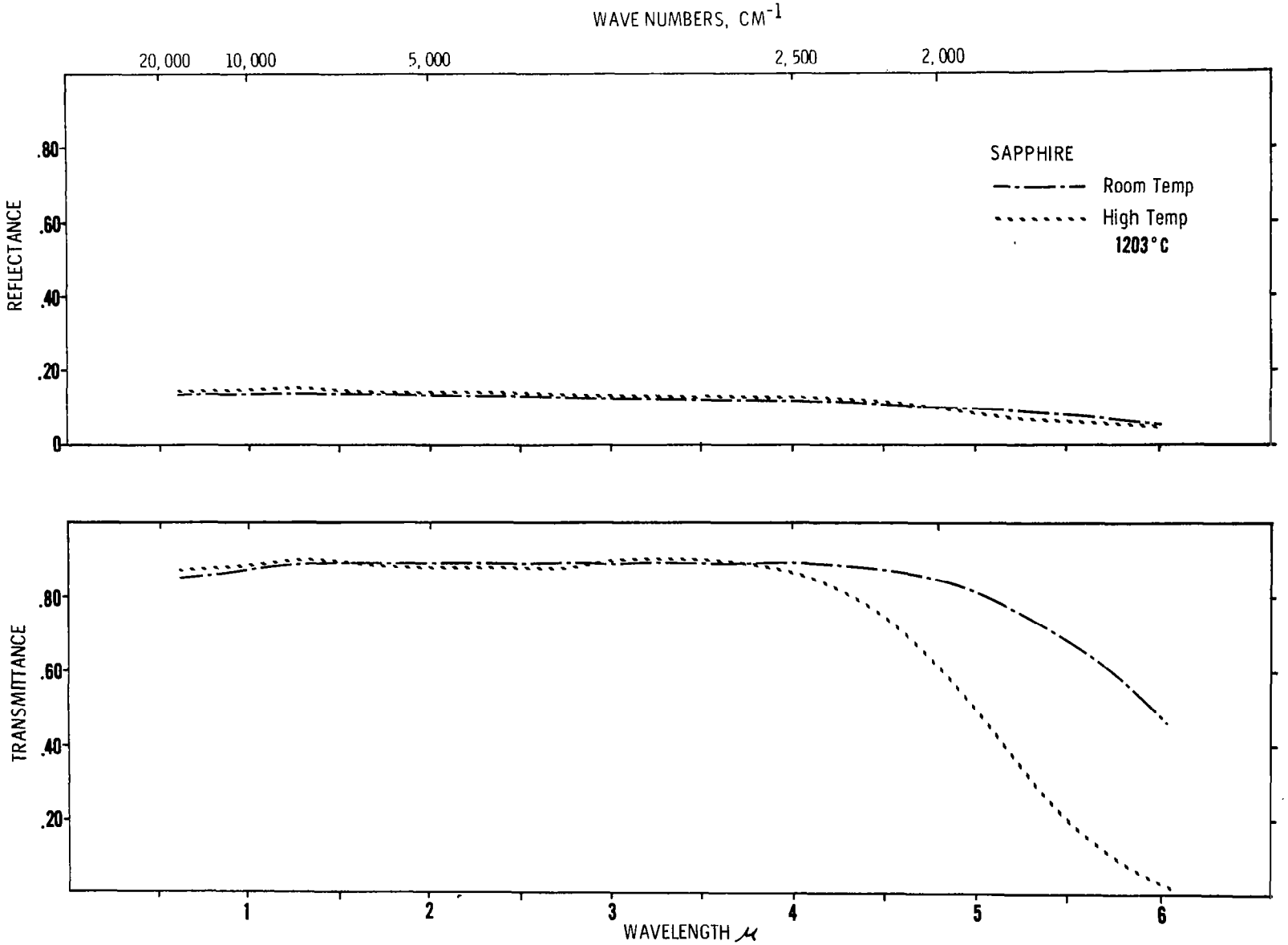

FIG. 20 TRANSMITTANCE AND REFLECTANCE OF SAPPHIRE

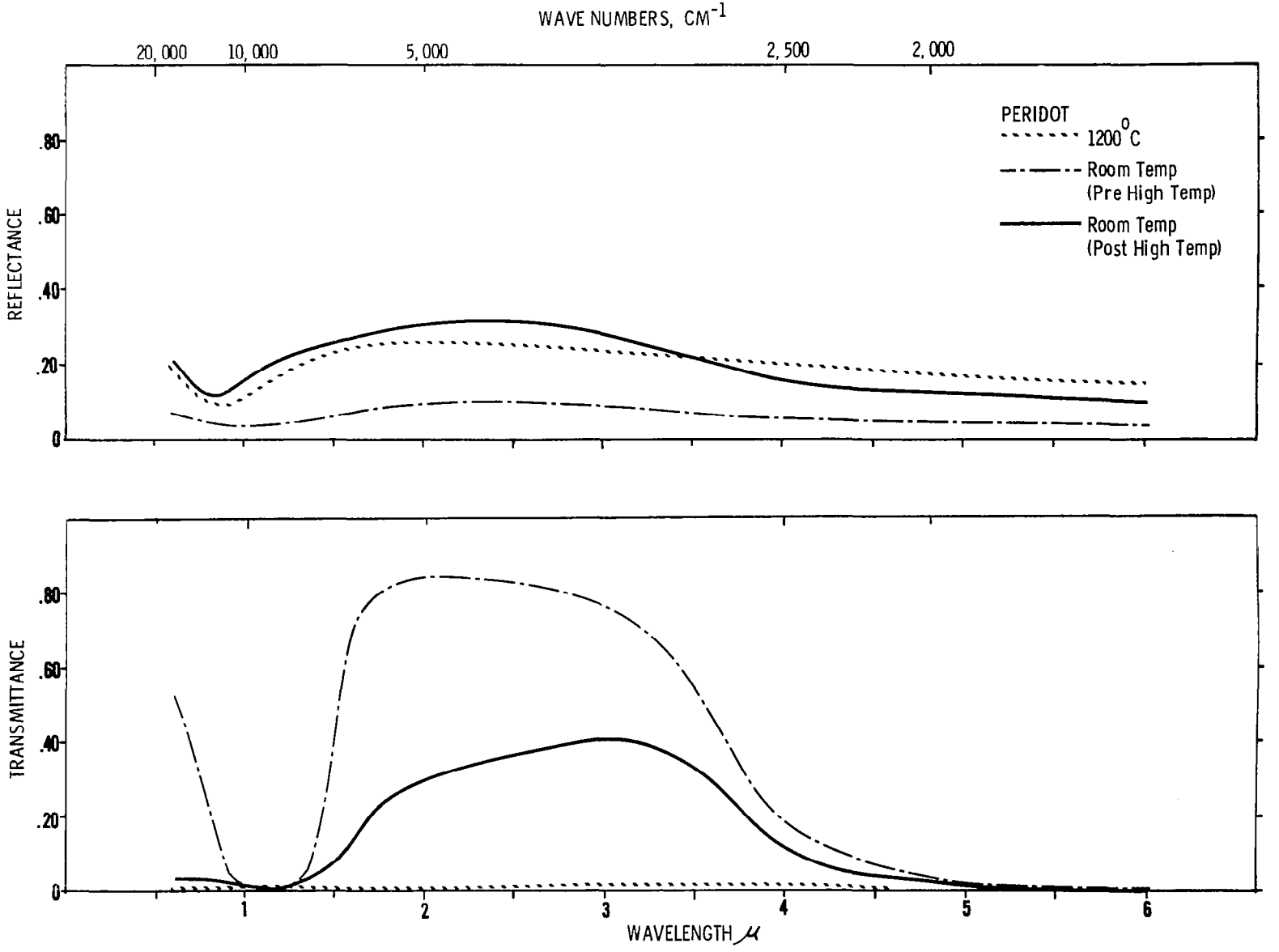

FIG. 21 TRANSMITTANCE AND REFLECTANCE OF PERIDOT

positions, and that color changes due to altered annealing atmospheres are due to changing valence states or locations of this smaller number of impurity ions.

When this crystal was heated to 1200°C it became opaque and the reflectance increased substantially. We reran the crystal at room temperature after cooling in order to ascertain how much of the changed properties might be ascribed to an irreversible change and how much to a strictly high temperature optical property change. The results are shown in Fig. 21. It can be seen that both effects occur. The extent to which radiation can be transmitted by the sample after cooling is probably an indication of a real temperature dependent effect as the sample is essentially opaque at high temperatures. The reduced level of transmission, however, indicates an irreversible change that was confirmed on visual examination. The surface was metallic in appearance but the thickness of the film was sufficiently small so that a yellow-golden color could be seen in transmitted light.

A small chip had fallen out of the crystal and it was magnetic although magnetism is not always apparent when the alteration occurs. Several attempts to identify this thin film by X-ray and electron diffraction techniques failed. The same thin film appears to occur when the material is heated in the open. When the material is crushed and heated, X-ray diffraction shows hematite and forsterite. We assume that the film has a composition near magnetite. Shankland [1966] has recorded seeing the same material and stated that some green translucence can be restored by reheating in hydrogen.

We repolished the original crystal and found that the principal attack was concentrated in a very thin surface layer. Mr. Cooley of A.D.Jones, Inc., indicated less than .001" had to be removed in repolishing the crystal. The crystal's color was then essentially recovered although a slight yellowing of the original green color may have occurred.

We ran a number of small peridot chips under conditions where oxidation should have been minimized, i.e., in high purity argon (in one case with a special assay of < 1.5 ppm of O_2, < 3 ppm H_2O, < 4 ppm N_2 and no

detectable hydrocarbons) to make certain that the tank actually contained its nominal impurity specifications. The attack occurred in every case demonstrating that the oxidation was not simply due to changing the furnace windows at temperature as was done in the original run to prevent window fogging. This practice was abandoned however and the low O_2 concentration in the argon seems to indicate that the oxidizing agent may have come from the ceramic tube. Finally, we learned to circumvent this problem by controlling the oxygen activity with an argon-1% hydrogen mixture that was passed through a source of H_2O vapor at 40°C [Bookey and Tombs, 1952]. The idea is to use a large excess of H_2O and H_2 to control the partial pressure of O_2 at about 10^{-9} atm. using the equilibrium

$$H_2O \rightleftarrows H_2 + O_2$$

The source of H_2O vapor is oxalic acid dihydrate. This method can be used in future runs on this mineral. The spectrum of peridot taken after the high temperature run indicates the formation of a long wavelength shoulder.

Diopside

The diopside crystal as previously mentioned was found to have a series of cracks running lengthwise in the colorless section. We therefore originally intended to run the green crack-free (and hence lower scattering) portion of the crystal. When we discovered the extent of the "oxidation" problem for the green peridot, we decided not to risk the green section of the diopside crystal and so determined to run the colorless section. In order to make a correction for scattering from the cracks we decided to run the green area at room temperature and to compare it with the room temperature spectrum of the colorless crystal also used for the high temperature studies. By using a part of the spectrum in which there is little or no absorption due to the iron that is responsible for the green coloration, we obtained a "non-scattering" transmission measurement that enabled us to correct the data for the colorless crystal to less scattering conditions. The correction used assumed that the

scattering is independent of wavelength in the relevant spectral region and neglects multiple reflections as being of minor importance in comparison with the other assumptions involved. The correction is obtained as follows. Using Eq. (68) under non-scattering conditions as:

$$\tau_o^* = (1 - r)^2 \, e^{-\alpha d}$$

and under scattering conditions:

$$\tau^* = (1 - r)^2 \, e^{-(\alpha+s)d} \tag{78}$$

where s is a scattering coefficient, one obtains

$$\frac{\tau_o^*}{\tau^*} = e^{sd} = A \tag{79}$$

when s is independent of wavelength and temperature. By using this constant, obtained from room temperature data from the green and colorless portions of the same crystal at wavelengths where there is no difference in α or r due to the green coloration material, we can correct the colorless crystal spectrum to a non-scattering situation.

During the heating of the diopside to high temperatures we observed an accentuation of the cracks with attendant increase in scattering. We are correcting for this change by the same method, by repeating our room temperature measurements after heating. The transmission and reflection data obtained at room temperature are shown in Fig. 22. It is easily seen that the scattering effects are in the correct direction in the three spectra. The scattering is, of course, more important in the transmission data than in the reflection data as all radiation removed from the incident beam by scattering appears as an apparent absorption. In the reflection

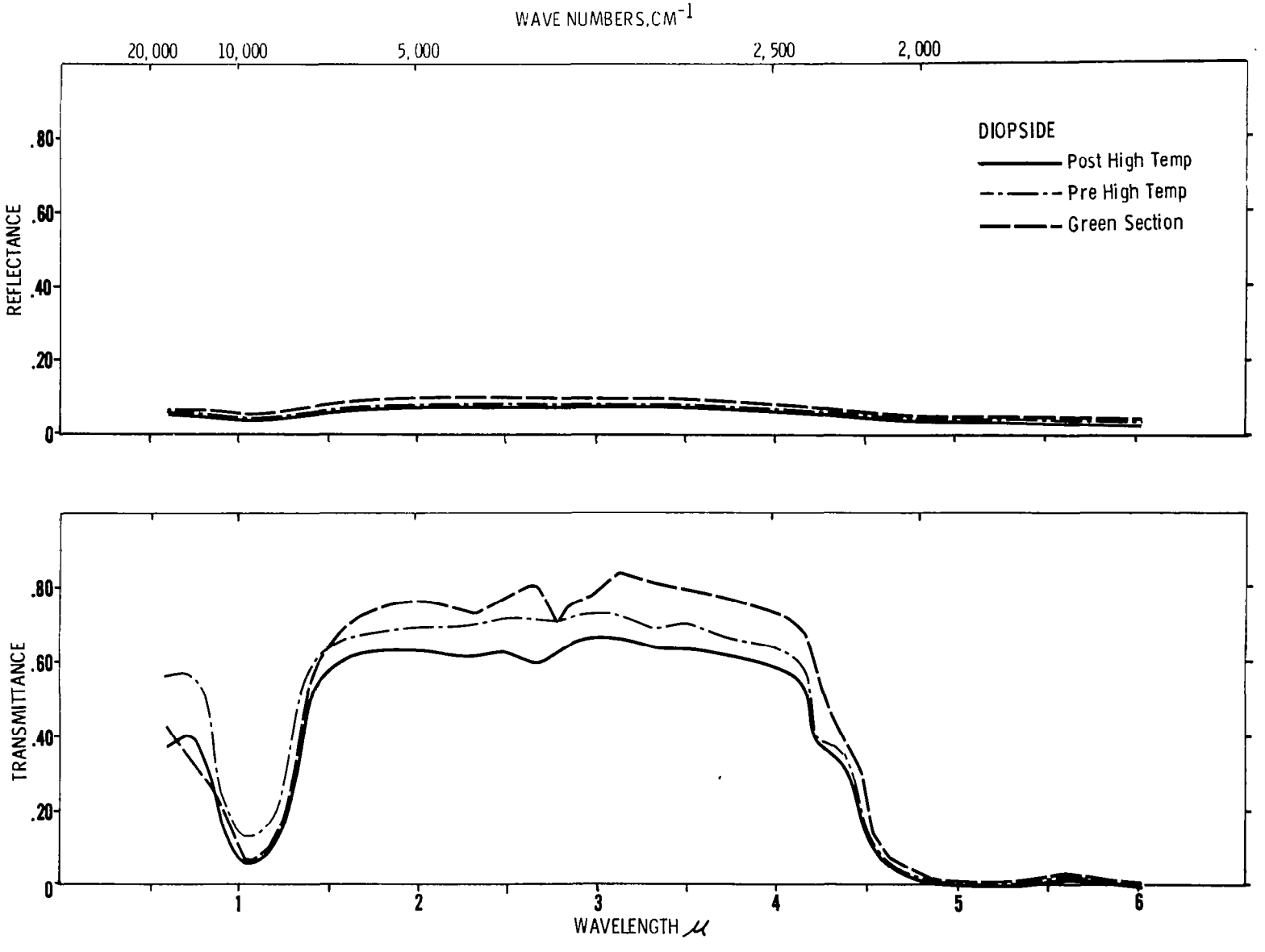

FIG. 22 TRANSMITTANCE AND REFLECTANCE OF DIOPSIDE AT ROOM TEMPERATURE

data, only that portion scattered directly backwards adds to the reflection. On the other hand, the portion removed from the beam by scattering is prevented from being reflected from the second surface (or, multiple bounces). A similar correction to that described above is made for the apparent reflectance.

It should be noted however, that even the green diopside at the peak of its transmission near 3.2μ, still has either some scattering or true absorption caused by the overlapping wings of bands, as $\tau^* + R^*$ does not sum to 1. We assume that this is true absorption.

A comparison of the spectra from the green and clear diopside areas is particularly interesting in the light of previous discussions of the origin of the green color in various crystals and glasses. White and Keester [1966] and Clark [1957b] have measured the spectrum of diopside and both observed a strong absorption feature centered near 1.08μ. As stated by White and Keester, this feature is due to ferrous iron in sixfold coordination as in other minerals. This absorption has also been ascribed to the ferrous iron in glass [Grove and Jellyman, 1955].

As with peridot, it is generally presumed that the green color of diopside is due to the tail of this band absorbing in the red. Comparison of the spectra of our colorless and green samples tends to indicate that the green color in our sample is rather due to the tail of the side band that appears as a shoulder near 0.7μ than to the tail of the main absorption. It is true that the main band is relatively stronger in the green sample as might be expected. The other noteworthy differences between the spectra of the green and colorless samples are the presence of a pronounced absorption at 2.77μ with a long wavelength shoulder and a broad absorption near 2.3μ for the green sample. White and Keester [1966] originally ascribed the broad-band at 4420 cm^{-1} (2.26μ) to ferrous iron in fourfold coordination but have recently decided otherwise [White, 1967]. The band at 2.77μ is probably due to water in the crystal as has been discussed for glasses [Grove and Jellyman, 1955] [Adams and Douglas, 1959], though these authors also ascribe a band at 2.2μ to water.

During the course of the high temperature runs, we had several experimental difficulties. These included a chopper breakdown and the reflectance glowbar burning out. As continuous calibrations and checks were run, we managed to salvage all the data except for the 1040°C reflectance. The high temperature reflectance and transmittance data are shown in Fig. 23 along with the room temperature data taken after cooling. These spectra clearly show the importance of using high temperature spectra in radiative transfer calculations in place of room temperature data. Both the long wavelength absorption due to the edge of the vibrational bands and the ferrous iron electronic transition band centered near 1.1μ broaden significantly with temperature. This leads to a significant increase in the absorption coefficient, even at wavelengths between the bands due to the overlap of the wings of both bands. It should be noted that there is no decrease in intensity at the ferrous band-center to compensate for the intensity increase in the wings.

In Fig. 24 we show the absorption coefficient derived from these measurements corrected for scattering as discussed previously. These data have been used to calculate the radiative conductivity shown in Table III. The spectra were used in the same way to calculate "approximate" radiative conductivity values at other high temperatures shown in the table

Oligoclase

The room temperature spectra are shown in Fig. 25. Once again spectra were measured before and after the high temperature run. The plan had been to make measurements just below and above the temperature at which the bubbles [Smith, 1963] disappeared in order to allow for scattering from them. After the room temperature data were obtained we proceeded to heat the crystal. Unfortunately a large crack appeared in the crystal directly in the optical path during heating to the vicinity of 400°C. We moved the crystal so as to make our measurements on an undamaged area and continued heating to 1030°C. Many further fractures occurred but the crystal retained its integrity so that high temperature measurements were made. We then returned to room temperature and repeated those measurements in order to be able to correct for the changes in scattering behavior

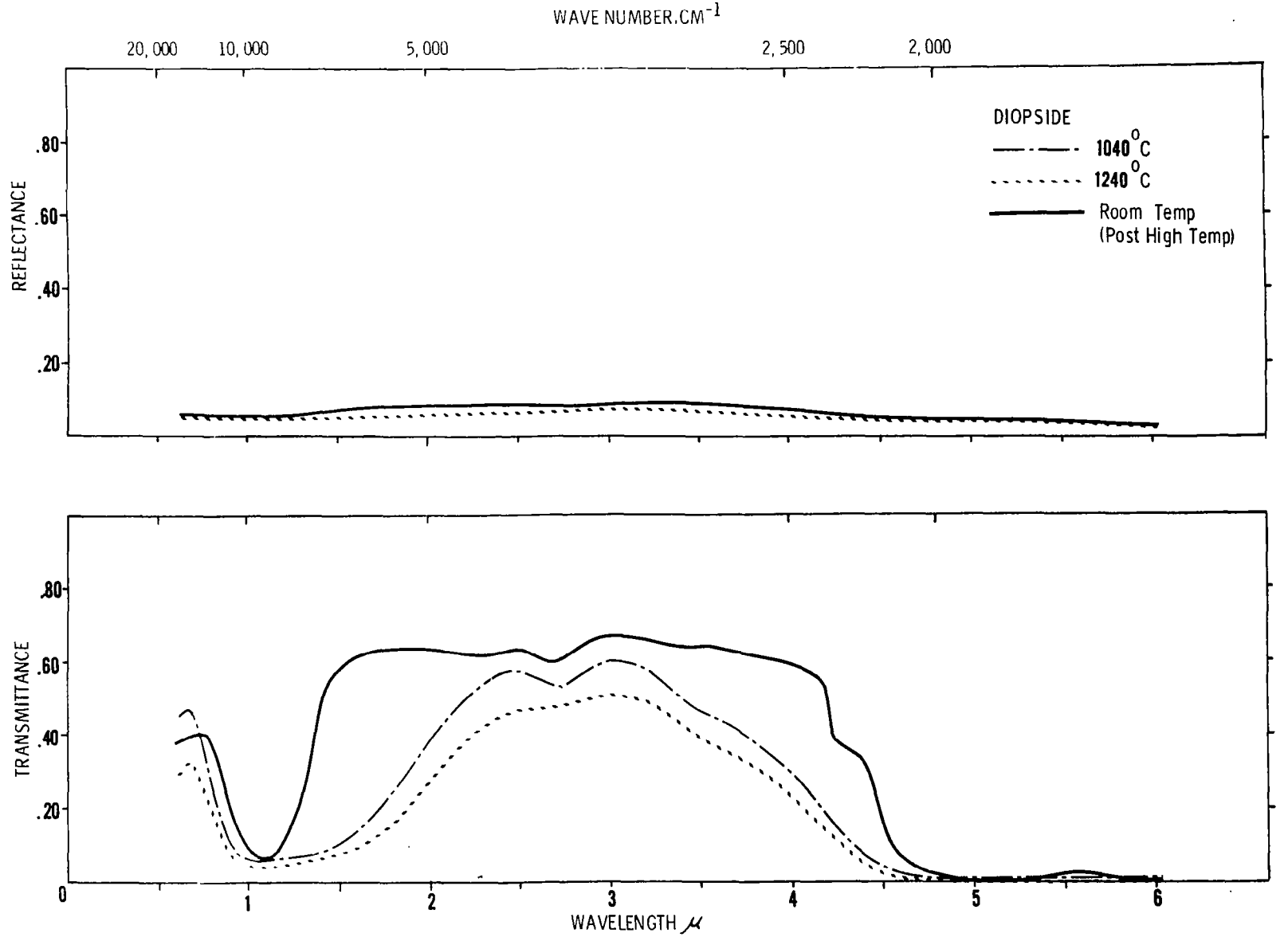

FIG. 23 TEMPERATURE DEPENDENCE OF THE TRANSMITTANCE AND REFLECTANCE OF DIOPSIDE

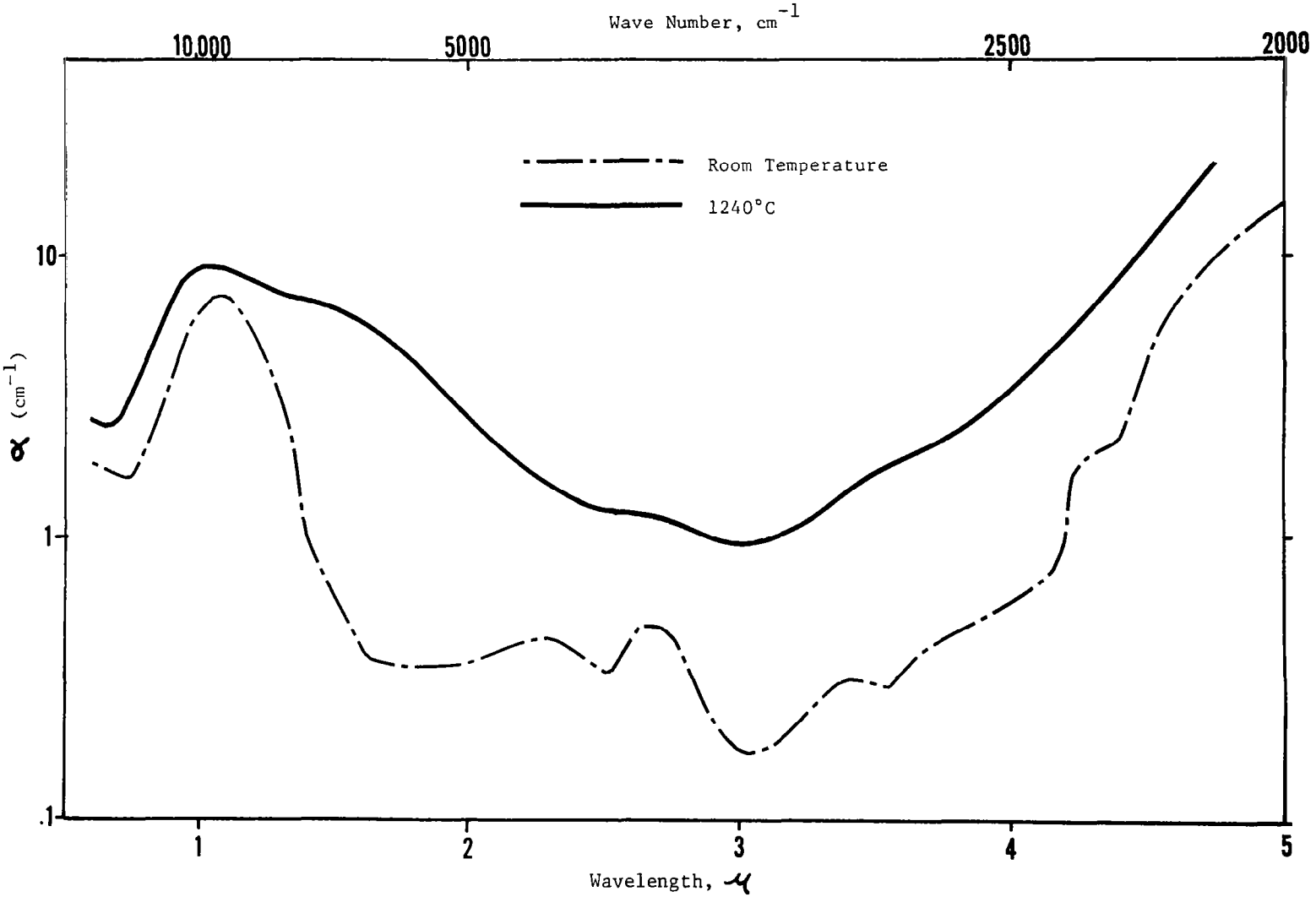

FIG. 24 ABSORPTION COEFFICIENT OF DIOPSIDE

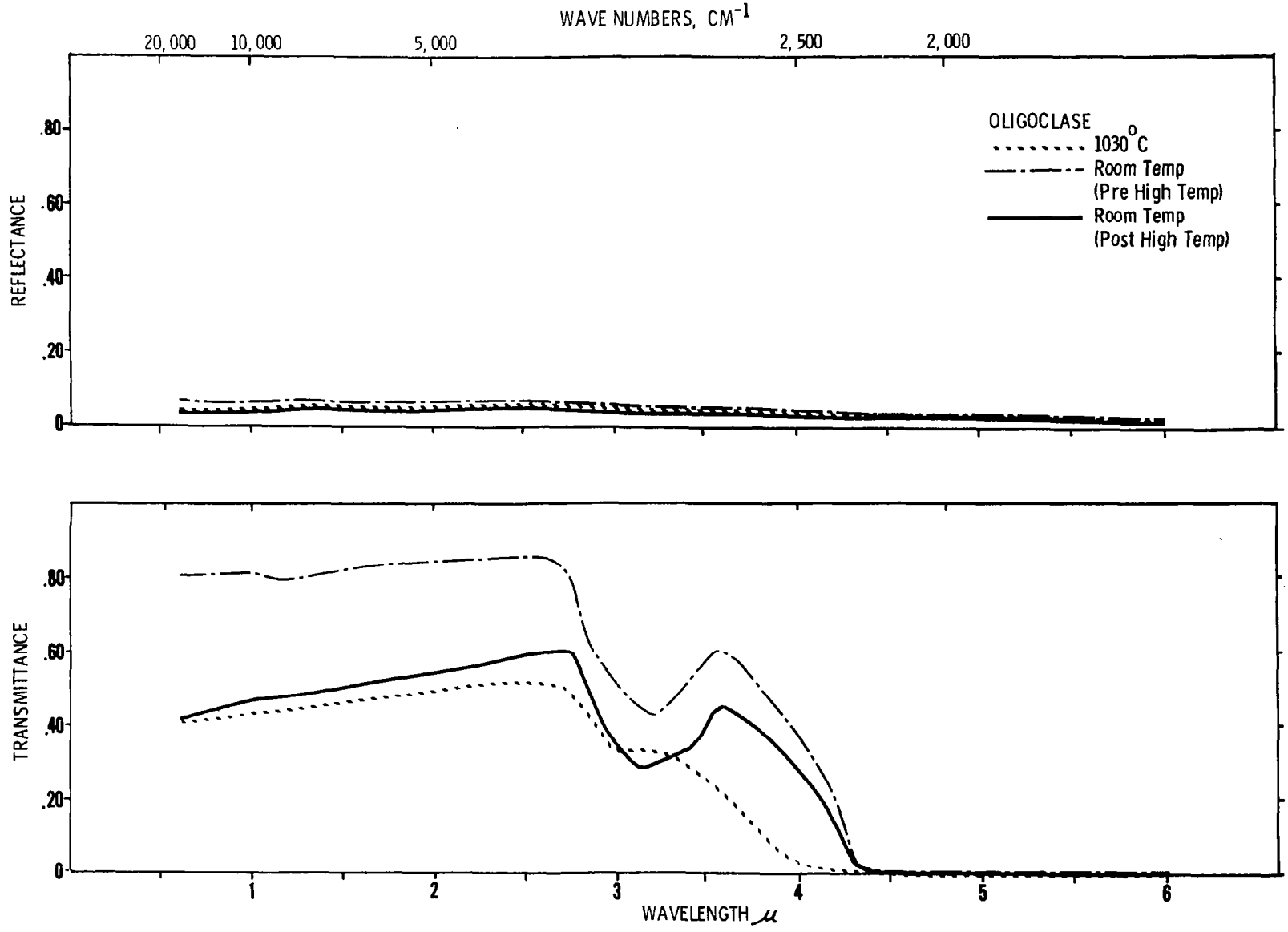

FIG. 25 TRANSMITTANCE AND REFLECTANCE OF OLIGOCLASE

of the sample. The 1030°C measurements are also shown in Fig. 25. As the crystal had been moved, considerable fracturing had occurred during heating and the original crystal contained a number of small bubbles, it is somewhat difficult to know precisely how to correct these spectra for scattering. We decided to apply the same kind of correction discussed previously using the room temperature data obtained prior to heating as "non-scattering." Visual examination of the original crystal and the fractured crystal suggest this as the best expedient. The "corrected" data was used to obtain the absorption coefficient shown in Fig. 26 and the radiative conductivities given in Table III.

Comparison of the high temperature data with that obtained at room temperature clearly shows the broadening of the vibrational bands toward shorter wavelengths as in previous cases. The other important feature is centered near 3.2μ for the room temperature data and near 3μ at 1030°C. These appear to be significantly displaced from bands reported due to H_2O of crystallization in feldspar [Saksena, 1961].

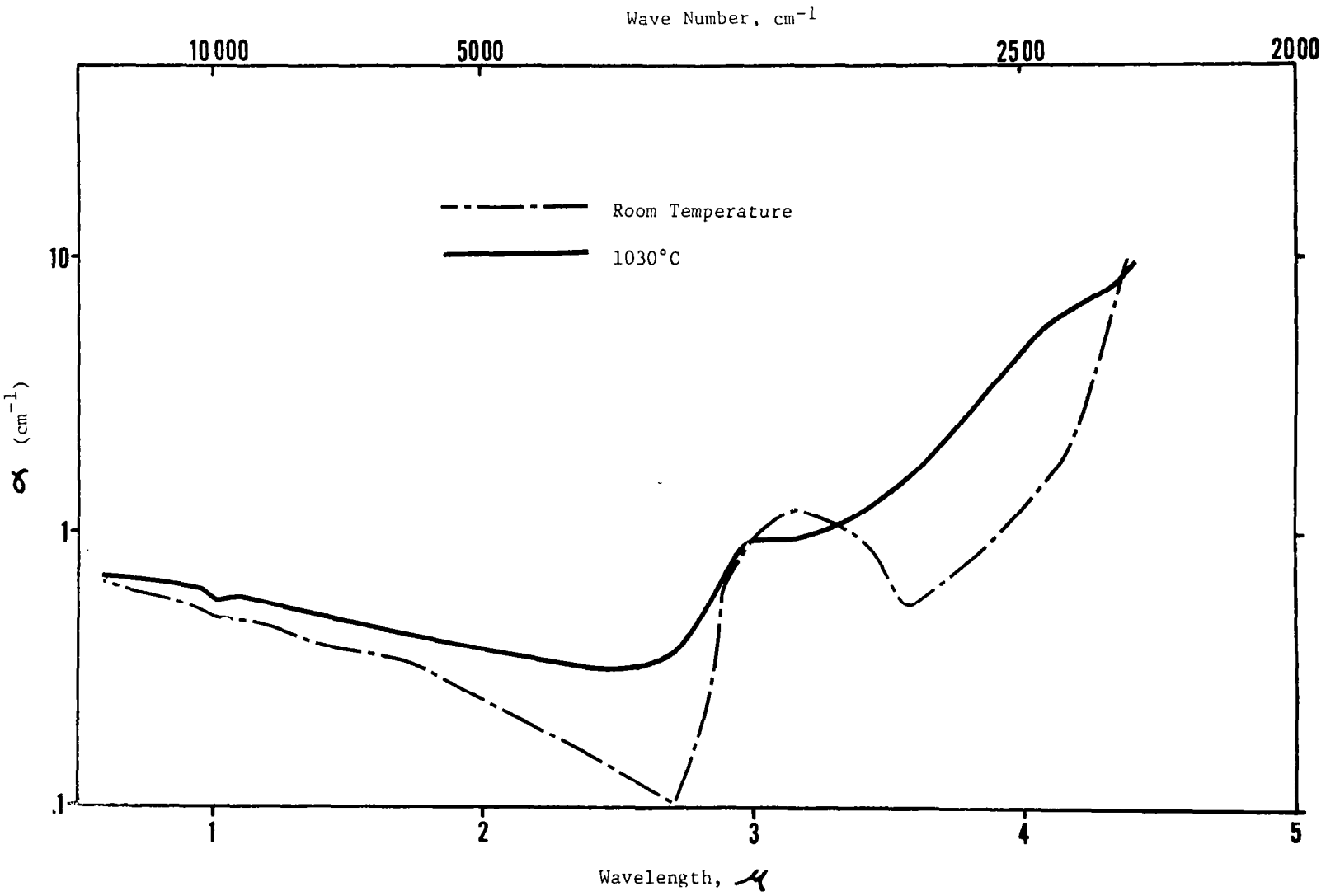

FIG. 26 ABSORPTION COEFFICIENT OF OLIGOCLASE

TABLE III

RADIATIVE CONDUCTIVITY (This Work)*

MINERAL	Temperature °K					
	1000		1303		1513	
	watts/cm°K	cal/cm sec°K	watts/cm°K	cal/cm sec°K	watts/cm°K	cal/cm sec°K
Diopside						
Using Room Temperature						
Spectral Data	.151	.0361	.349	.0834	.516	.123
Using 1513°K						
Spectral Data	.032	.0076	.0705	.0168	.102	.0244
Oligoclase						
Using Room Temperature						
Spectral Data	.156	.0373	.425	.102		
Using 1303°K						
Spectral Data	.0877	.0210	.255	.0606		

*All results corrected for scattering behavior as described in text.
Integration from .60μ to 5.82μ.

XII. IMPLICATIONS OF THERMAL CONDUCTIVITY DATA FOR LUNAR THERMAL HISTORY AND HEAT FLOW

It is clear from the above results that our suspicions that earlier estimates of thermal conductivity at high temperature based on room temperature data might be seriously in error were well founded. Our preliminary results indicate that an increase in absorption coefficient with temperature, as expected, occurs in rock-forming minerals both with and without iron. Our best data are those for diopside from which radiative thermal conductivities at 1513°K calculated from the high temperature spectra are only 1/5 of the value calculated from room temperature spectra. In our previous report it was noted that a factor of three in thermal conductivity could make the difference between melting and not melting within the moon. Shoemaker [private communication] has recently suggested that many of the lunar maria are relatively young. As we showed that volcanic activity could occur late in the moon's history only for very low thermal conductivities and relatively low concentrations of radioactive heat sources compared to those generally accepted for the moon or the earth, the preliminary data on diopside and plagioclase would seem to indicate that effects of temperature are in the right direction. If olivine and other upper mantle minerals behave similarly, a consistent picture of the thermal history of the moon would seem to be within reach. If Shoemaker's dating of the maria is correct, and if further work on the spectra of minerals substantiates our above conclusions, then lunar radioactivity and heat flow may be considerably less than estimated by most other workers. This point will be discussed in more detail in the final report for Contract NAS9-5839.

XIII. SUGGESTIONS FOR FURTHER WORK

As anticipated, we have spent considerable time in setting up and refining the apparatus for measuring high temperature mineral spectra. The first few minerals have indicated the kind of results to be expected. We feel that the relative effects we have measured are more reliable than the precise numbers obtained particularly because of the problem of correcting the data for changes in scattering behavior on temperature cycling.

We believe that the apparatus we have developed should be used to make a series of measurements on a number of different mineral samples and at different crystal orientations. This would greatly improve the reliability of the numbers obtained. We also believe it would be most valuable to extend the temperature range upwards and to include measurements through the melting temperature. Our apparatus was so designed that this could be accomplished with a minimum amount of effort, using a platinum cup with polished bottom for molten samples.

The theory of scattering as presently developed is badly in need of experimental checks. We would propose to carry some out by means of both thermal conductivity and optical measurements on model systems.

Finally, we believe it would be valuable to extend our random orientation interface model to include absorption in a similar way to that used in the plane layer Fresnel reflection model. This would become important if the mantle really consists of crystallites much smaller than about 1 mm.

REFERENCES

Adams, R.V., and Douglas, R.W., Infra-red studies of various samples of fused silica with special reference to the bands due to water, Trans. Soc. Glass Technology 43, 147-158, 1959.

Bennett, J.M., and Ashley, E.J., Infrared Reflectance and Emittance of Silver and Gold Evaporated in Ultrahigh Vacuum, Appl. Opt. 4, 221-224, 1965.

Bookey, J.B., and Tombs, N.C., Oxalic Acid Dihydrate as a Source of Low Water-Vapour Pressure, J. Iron Steel Inst. 172, 86, 1952.

Clark, S.P., Jr., Radiative Transfer in the Earth's Mantle, Trans. Amer. Geophys. Union 38, 931-938, 1957a.

Clark, S.P., Jr., Absorption Spectra of Some Silicates in the Visible and Near Infrared, Amer. Mineralogist 42, 732-742, 1957b.

Czerny, M., and Genzel, L., Energiefluss and Temperatur verlauf in Glasbad von Schmerzwannen als Folge von Wärmeleitung und Wärmestrahlung, Glastech. Ber. 25, 387-392, 1952.

Duntley, S.Q., The Optical Properties of Diffusing Materials, 32, 61-70, 1942.

Farrell, E.G., and Newnham, R.E., Amer. Mineralogist 50, 1972-1981, 1965.

Gardon, R., A Review of Radiant Heat Transfer in Glass, J. Am. Ceram. Soc. 44, 305-312, 1961.

Genzel, L., Messung der Ultrarot-Absorption von Glas Zwischen 20 und 1360°C, Glastechn. Ber. 24, 55-63, 1951.

Grove, F.J., and Jellyman, P.E., The Infra-Red Transmission of Glass in the Range Room Temperature to 1400°, Trans. Soc. Glass Technology 39, 3-15, 1955.

Gryvnak, D.A., and Burch, D.E., Optical and infrared properties of Al_2O_3 at elevated temperatures, J. Opt. Soc. Am. 55, 625-629, 1965.

Kellett, B.S., The Steady Flow of Heat Through Hot Glass, J. Opt. Soc. Am. 42, 339-343, 1952.

Kubelka, P., New Contributions to the Optics of Intensely Light-Scattering Materials I, J. Opt. Soc. Am. 38, 448-457, 1948.

Lee, D.W., and Kingery, W.D., Radiation energy transfer and thermal conductivity of ceramic oxides, J. Am. Ceram. Soc. 42, 594-607, 1960.

MacDonald, G.J.F., Calculations on the Thermal History of the Earth, J. Geophys. Res. 64, 1967-2000, 1959.

McConnell, R.K., Allen, R.V., Aronson, J., Feick, G., Lee, D.W., McClaine, L., and Vonnegut, B., The Effect of the Lunar Environment on Magma Generation, Migration and Crystallization, A. D. Little, Inc., Final Report on Contract NAS9-3449 to NASA Manned Spacecraft Center, Nov. 1965.

McConnell, R.K., Jr., McClaine, L.A., Lee, D.W., Aronson, J.R., and Allen, R.V., A Model for Planetary Igneous Differentiation, Rev. Geophys., in press, May 1967.

McMahon, H.O., Thermal Radiation from Partially Transparent Reflecting Bodies, J. Opt. Soc. Am. 40, 376-380, 1950

Neuroth, N., Der Einfluss der Temperatur auf die spektrale Absorption von Gläsern in Ultraroten, Glastechn. Ber. 25, 242-249, 1952.

Saksena, B.D., Infra-Red Absorption Studies of Some Silicate Structures, Trans. Far. Soc. 57, 242-255, 1961.

Schuster, A., Radiation Through a Foggy Atmosphere, Astrophys. J. 21, 1, 1905.

Shankland, T.J., Synthesis and Optical Properties of Forsterite, Office of Naval Research Technical Report No. HP-16, July 1966.

Smith, F.G., Physical Geochemistry, pp. 509ff, Addison-Wesley, Reading, Mass., 1963.

Wegge, L., On a Discrete Version of the Newton Raphson Method, Siam J. on Numerical Analysis 3, 134-142, 1966.

White, W.B., and Keester, K.L., Optical Absorption Spectra of Iron in the Rock-Forming Silicates, Amer. Mineralogist 51, 774-791, 1966.

White, W.B., Correlation of Optical Spectra with Structural Environment of Fe^{++} in Pyroxenes, paper presented at 48th Annual Meeting of the A.G.U., April 18, 1967, Washington, D.C.

"The aeronautical and space activities of the United States shall be conducted so as to contribute . . . to the expansion of human knowledge of phenomena in the atmosphere and space. The Administration shall provide for the widest practicable and appropriate dissemination of information concerning its activities and the results thereof."

—NATIONAL AERONAUTICS AND SPACE ACT OF 1958

NASA SCIENTIFIC AND TECHNICAL PUBLICATIONS

TECHNICAL REPORTS: Scientific and technical information considered important, complete, and a lasting contribution to existing knowledge.

TECHNICAL NOTES: Information less broad in scope but nevertheless of importance as a contribution to existing knowledge.

TECHNICAL MEMORANDUMS: Information receiving limited distribution because of preliminary data, security classification, or other reasons.

CONTRACTOR REPORTS: Scientific and technical information generated under a NASA contract or grant and considered an important contribution to existing knowledge.

TECHNICAL TRANSLATIONS: Information published in a foreign language considered to merit NASA distribution in English.

SPECIAL PUBLICATIONS: Information derived from or of value to NASA activities. Publications include conference proceedings, monographs, data compilations, handbooks, sourcebooks, and special bibliographies.

TECHNOLOGY UTILIZATION PUBLICATIONS: Information on technology used by NASA that may be of particular interest in commercial and other non-aerospace applications. Publications include Tech Briefs, Technology Utilization Reports and Notes, and Technology Surveys.

Details on the availability of these publications may be obtained from:

SCIENTIFIC AND TECHNICAL INFORMATION DIVISION

NATIONAL AERONAUTICS AND SPACE ADMINISTRATION

Washington, D.C. 20546